

AD-A246 136



U.S. NAVAL POSTGRADUATE SCHOOL  
Monterey, California

2



THESIS

DTIC  
SELECTED  
FEB 20 1992  
SBD

EFFECT OF THERMAL RESIDUAL STRESSES  
ON THE STRESS-STRAIN BEHAVIOR  
OF METAL-MATRIX COMPOSITES

by

Daniel M. Seigenthaler

JUNE 1991

Thesis Advisor:

I. Dutta

Approved for public release: Distribution is unlimited

92-03685



92 2 12 162

## Unclassified

## SECURITY CLASSIFICATION OF THIS PAGE

REPORT DOCUMENTATION PAGE				Form Approved OMB No 0704-0188
1a. REPORT SECURITY CLASSIFICATION Unclassified		1b. RESTRICTIVE MARKINGS		
2a. SECURITY CLASSIFICATION AUTHORITY		3. DISTRIBUTION/AVAILABILITY OF REPORT Approved for public release: Distribution is unlimited		
2b. DECLASSIFICATION/DOWNGRADING SCHEDULE				
4. PERFORMING ORGANIZATION REPORT NUMBER(S)		5. MONITORING ORGANIZATION REPORT NUMBER(S)		
6a. NAME OF PERFORMING ORGANIZATION Naval Postgraduate School	6b. OFFICE SYMBOL <i>(If applicable)</i> ME	7a. NAME OF MONITORING ORGANIZATION Naval Postgraduate School		
8c. ADDRESS (City, State and ZIP Code)  Monterey, CA 93943-5000		7b. ADDRESS (City, State, and ZIP Code)  Monterey, CA 93943-5000		
8a. NAME OF FUNDING/SPONSORING ORGANIZATION	8b. OFFICE SYMBOL <i>(If applicable)</i>	9. PROCUREMENT INSTRUMENT IDENTIFICATION NUMBER		
8c. ADDRESS (City, State, and ZIP Code)		10. SOURCE OF FUNDING NUMBER		
		PROGRAM ELEMENT NO.	PROJECT NO.	TASK NO.
11. TITLE (Include Security Classification)  EFFECT OF THERMAL RESIDUAL STRESSES ON THE STRESS-STRAIN BEHAVIOR OF METAL-MATRIX COMPOSITES				
12. PERSONAL AUTHORS DANIEL M. SEIGENTHALER				
13a. TYPE OF REPORT Master's Thesis	13b. TIME COVERED FROM _____ TO _____	14. DATE OF REPORT (Year, Month, Day) JUNE 1991		15. PAGE COUNT 91
16. SUPPLEMENTARY NOTATION The views expressed are those of the author and do not reflect the official policy or position of the Department of Defense or the U.S. Government				
17. COSATI CODES		18. SUBJECT TERMS (Continue on reverse if necessary and identify by block numbers) thermal stresses, composites, finite element		
FIELD	GROUP			
19. ABSTRACT (Continue on reverse if necessary and identify by block numbers)  A phenomenological and parametric study was conducted to assess the effect of thermal residual stresses on the stress-strain response of a discontinuous fiber-reinforced metal-matrix composite in tensile and compressive loading. The material chosen for this investigation was the SiC-whisker reinforced Al 6061. The difference between composite flow behavior in tension and compression, as well as the effects of volume fraction, fiber aspect ratio and fiber spacing were analyzed within the framework of axisymmetric finite-element models to determine the overall constitutive response of the composite and to solve for local field quantities in the fiber and the matrix. The composite was modeled as a periodic array of cylindrical fibers with perfect interfacial bonding and complete fiber alignment with the tensile/compressive axis. It was found that the presence of residual stresses affected the stress-strain behavior of the composite by influencing the load transfer characteristics between the matrix and the fiber as well as the initiation and growth of the plastic deformation in the matrix. The results of the study indicated that a significant strength differential exists between tensile and compressive loading and that this effect diminishes with increasing volume fraction. The results also indicated that composite stiffness, yield strength and work-hardening rate increase with increasing volume fraction and fiber aspect ratio and that the variation in fiber spacing has a relatively small effect in tension and a large effect in compression due to the presence of residual stresses.				
20. DISTRIBUTION/AVAILABILITY OF ABSTRACT <u>XX UNCLASSIFIED/UNLIMITED</u> <u>SAME AS RPT</u> <u>DTIC USERS</u>		21. ABSTRACT SECURITY CLASSIFICATION Unclassified		
22a. NAME OF RESPONSIBLE INDIVIDUAL I. Dutta		22b. TELEPHONE (Include Area Code) (408) 646-2851	22c. OFFICE SYMBOL ME/Du	

Approved for public release: Distribution is unlimited

Effect of Thermal Residual Stresses  
on the Stress-Strain Behavior  
of Metal-Matrix Composites

by

Daniel M. Seigenthaler  
Lieutenant, United States Navy  
B.S., United States Naval Academy

Submitted in partial fulfillment of the  
requirements for the degree of

MASTER OF SCIENCE  
IN MECHANICAL ENGINEERING

from the

NAVAL POSTGRADUATE SCHOOL

JUNE 1991

Author:



\_\_\_\_\_  
Daniel M. Seigenthaler

Approved by:



\_\_\_\_\_  
I. Dutta, Thesis Advisor



\_\_\_\_\_  
Anthony J. Healy, Chairman

Department of Mechanical Engineering

## **ABSTRACT**

A phenomenological and parametric study was conducted to assess the effect of thermal residual stresses on the stress-strain response of a discontinuous fiber-reinforced metal-matrix composite in tensile and compressive loading. The material chosen for this investigation was the SiC-whisker reinforced Al 6061. The difference between composite flow behavior in tension and compression, as well as the effects of volume fraction, fiber aspect ratio and fiber spacing were analyzed within the framework of axisymmetric finite-element models to determine the overall constitutive response of the composite and to solve for local field quantities in the fiber and the matrix. The composite was modeled as a periodic array of cylindrical fibers with perfect interfacial bonding and complete fiber alignment with the tensile/compressive axis. It was found that the presence of residual stresses affected the stress-strain behavior of the composite by influencing the load transfer characteristics between the matrix and the fiber as well as the initiation and growth of the plastic deformation in the matrix. The results of the study indicated that a significant strength differential exists between tensile and compressive loading and that this effect diminishes with increasing volume fraction. The results also indicated that composite stiffness, yield strength and work-hardening rate increase with increasing volume fraction and fiber aspect ratio and that the variation in fiber spacing has a relatively small effect in tension and a large effect in compression due to the presence of residual stresses.

Accession For	
NTIS GRA&I	<input checked="" type="checkbox"/>
DTIC TAB	<input type="checkbox"/>
Unannounced	<input type="checkbox"/>
Justification	
By _____	
Distribution/	
Availability Codes	
Avail and/or Dist	Special
A-1	

## TABLE OF CONTENTS

I.	INTRODUCTION AND LITERATURE SEARCH . . . . .	1
	A. THERMAL RESIDUAL STRESSES IN METAL-MATRIX COMPOSITES . . . . .	1
	B. STRESS-STRAIN BEHAVIOR OF METAL MATRIX COMPOSITES . . . . .	4
	C. STRENGTH DIFFERENTIAL EFFECT . . . . .	6
	D. RESEARCH OBJECTIVES AND OVERVIEW . . . . .	8
II.	EXPERIMENTAL APPROACH . . . . .	10
	A. NUMERICAL MODELING . . . . .	10
	1. Finite Element Modeling . . . . .	10
	2. Boundary Conditions . . . . .	13
	3. Applied loading . . . . .	13
	4. Grid Independence . . . . .	14
	5. Model Implementation . . . . .	15
	B. MATERIAL TESTING . . . . .	16
III.	RESULTS . . . . .	18
	A. EFFECTS OF THERMAL RESIDUAL STRESSES: A PHENOMENOLOGICAL STUDY . . . . .	18
	1. Constitutive Composite Response . . . . .	18
	2. Plastic Zone Initiation and Growth: Von Mises Effective Stress . . . . .	22
	3. Cumulative Effective Plastic Strain . . .	27
	4. Fiber Loading in Tension and Compression . . . . .	29
	5. Axial Stresses in the Composite . . . . .	32
	6. Hydrostatic Stresses in the Composite . .	36
	B. PARAMETRIC STUDY . . . . .	40
	1. Fiber Volume Fraction Effects . . . . .	40
	a. Stress-Strain Behavior . . . . .	40
	b. Plastic Zone Initiation and Growth . . . . .	46
	c. Effective Plastic Strain . . . . .	48
	d. Fiber Loading . . . . .	48

e. Hydrostatic Stress . . . . .	54
2. Fiber Aspect Ratio Effects . . . . .	56
a. Stress-Strain Behavior . . . . .	56
b. Fiber Loading Rate Behavior . . . .	56
3. Cell Aspect Ratio Effects . . . . .	58
C. EXPERIMENTAL RESULTS . . . . .	59
IV. CONCLUSIONS . . . . .	65
A. EFFECT OF THERMAL RESIDUAL STRESSES . . . . .	65
B. PARAMETRIC STUDY . . . . .	66
APPENDIX A: SAMPLE ADINA INPUT FILE . . . . .	67
APPENDIX B: DATA REDUCTION PROGRAMS . . . . .	71
LIST OF REFERENCES . . . . .	76
INITIAL DISTRIBUTION LIST . . . . .	78

## LIST OF FIGURES

Figure 1.	Material Representation: Diagram Showing (a) the Aligned Fiber Arrangement and (b) a Depiction of the Fiber Imbedded in the Matrix Shell. . . . .	12
Figure 2.	Residual Stress Effects: Effects of Thermal Residual Stresses (TRS) in Tension and Compression. (a) Composite Stress-Strain Behavior and (b) Fiber and Matrix Stress-Strain Behavior. . . . .	19
Figure 3.	Plastic Zone Development-Von Mises Effective Stress in Tension: Contours of Effective Stress for a 10 vol.% MMC ( $A_f=A_c=6$ ) With and Without Residual Stress. . . . .	23
Figure 4.	Plastic Zone Development-Von Mises Effective Stress in Compression: Contours of Effective Stress for a 10 vol.% MMC ( $A_f=A_c=6$ ) With and Without Residual Stress. . . . .	26
Figure 5.	Cumulative Effective Plastic Strain: Effective Plastic Strain for a 10 vol.% MMC with $A_f=A_c=6$ at an Equivalent Value of Strain ( $\epsilon_c=0.010$ ) in Tension With Residual Stresses, Compression With Residual Stresses, and Tension/Compression Without Residual Stresses. . . . .	28



Figure 13. Fiber Volume Fraction Effects: (a) Schematic of Model Configurations for Volume Fractions of 1.0%, 20% and 30% with $A_f=A_c=6$ and (b) Composite Stress-Strain Behavior MMC With Residual Stresses in Tension and Compression. . . . .	41
Figure 14. Fiber Volume Fraction Effects With and Without Residual Stresses: Composite Stress-Strain Curves in Tension and Compression for MMC with $A_f=A_c=6$ and Fiber Volume Fraction of (a) 10%, (b) 20% and (c) 30% . . . . .	43
Figure 15. Fiber Volume Fraction Effects in Fiber and Matrix: Fiber and Matrix Stress-Strain Behavior With and Without Residual Stresses in Tension and Compression for Fiber Volume Fractions of (a) 10% and (b) 30%. . . . .	45
Figure 16. Fiber Volume Fraction Effects - Plastic Zone Development: Von-Mises Effective Stress of 30 vol.% MMC With Residual Stresses in (a) Tension and (b) Compression. . . . .	47
Figure 17. Cumulative Effective Plastic Strain: Effective Plastic Strain at Equivalent Values of Composite Strain ( $\epsilon_c=0.010$ ) in Tension with TRS, Compression With TRS, and Tension/Compression Without TRS for (a) 10 vol.% MMC and (b) 30 vol.% MMC with $A_f=A_c=6$ . . . . .	49
Figure 18. Axial Fiber Stress With Residual Stresses: Axial Stress Carried by the Fiber at Indicated Composite Strains at Right in (a) 10 vol.% MMC and (b) 30 Vol.% MMC. . . . .	50

Figure 19.	Axial Fiber Stress 30 vol.% MMC With and Without Residual Stresses: Axial Stress Carried by the Fiber in (a) Tension and (b) Compression. . . . .	52
Figure 20.	Incremental Fiber Tip Stresses With and Without Residual Stress: Incremental Fiber-Tip Stress ( $\sigma_{zz,tip}/\Delta\varepsilon_c$ ) for Indicated Stress Regimes in (a) 10 vol.% MMC and (b) 30 vol.% MMC. . . . .	53
Figure 21.	Hydrostatic Stress for a 30 vol.% MMC: Contours of Hydrostatic Stress With Residual Stresses for a 30 vol.% in (a) Tension and (b) Compression. . . . .	55
Figure 22.	Fiber Aspect Ratio Effects: (a) Schematic of Model Configuration for 30 vol.% MMC with $A_f=A_c=10, 6, 3,$ and 1, and (b) Composite Stress-Strain Behavior in Tension and Compression in the Presence of Residual Stresses. . . . .	57
Figure 23.	Fiber Load-Bearing Behavior: Effect of Fiber Aspect Ratio and Volume Fraction on the Stress Carried by the Fiber with Residual Stresses. . . . .	58
Figure 24.	Fiber Spacing Effects: (a) Schematic of Fiber Spacing Models With $A_f=5$ and $A_c=3, 5,$ and 10, and (b) Composite Stress-strain Behavior in Tension and Compression with Residual Stresses. . . . .	60
Figure 25.	SEM Micrograph: Scanning Electron Microscopy Photography at 3,45 KX of a 30 vol.% SiC Fiber-Reinforced Al 6061 Composite With a 6.5:1 Reduction Ratio. . . . .	61

Figure 26. Experimental Testing Results:  
Comparison of Experimental Testing  
and Numerical Results in (a) Tensile  
Loading and (b) Tensile and  
Compressive Loading With Plastic  
Strain on the Horizontal Axis. . . . . 63

### **THESIS DISCLAIMER**

The reader is cautioned that computer programs utilized in this research may not have been exercised for all cases of interest. While every effort has been made, within the time available, to ensure that the programs are free from computational and logic errors, they cannot be considered validated. Any application of these programs without additional verification is at the risk of the user.

## **ACKNOWLEDGEMENT**

The author would like to express his appreciation to three individuals whose assistance was vital to the completion of this thesis. First, I would like to thank Professor Dutta for his guidance and patience, both as an instructor and an advisor. I would like to thank John Sims for his thorough, quality achievement developing the ADINA programs, as well as the long hours he spent teaching me the ropes, which lead to the continuation of the research. His early tensile results and extensive background investigation laid the framework for this follow-on study. Finally, I would like to thank my wife Carrie, who patiently endured nearly three years of long nights and no weekends. Without her never-ending support and encouragement, none of this would have been possible.

## **I. INTRODUCTION AND LITERATURE SEARCH**

In the last decade, advancements in fabrication technology have brought discontinuous fiber reinforced metal matrix composites to the lead in the search for the ever stiffer and stronger yet lighter and cheaper material. The addition of silicon carbide whiskers to an aluminum 6061 matrix through a powder metallurgy process is one of these commercially practical materials. It is both machinable and workable with conventional metal-forming techniques and can be produced in economically feasible quantities. It is a proven composite with routine applications that include automotive engine components, such as aluminum pistons with selective reinforcement and pure composite connecting rods. Improvements in mechanical properties over the unreinforced alloy include increased elastic modulus, tensile strength, wear resistance, fatigue resistance, and strength-to-weight ratio. In order for industry to utilize this material and similar metal matrix composites to their full potential detailed knowledge of the factors and mechanisms affecting their thermal, electrical and mechanical properties must be known.

### **A. THERMAL RESIDUAL STRESSES IN METAL-MATRIX COMPOSITES**

During fabrication of the metal matrix composite, a coefficient of thermal expansion (CTE) mismatch between the

matrix and the reinforcing fiber produces thermal residual stresses. The exact nature of these stresses and their effect on the mechanical properties of the composite has been the subject of many investigations. Early studies [Refs. 1, 2, 3, 4, 5, 6], used continuum mechanics to investigate thermal residual stress states in spherical particle reinforced MMCs, and in continuous fiber MMCs.

Arsenault et al. [Ref. 7, 8, 9, 10] used electron microscopy and X-ray diffraction to conclude that the residual stresses were caused by CTE mismatch and that matrix strengthening was due to enhanced dislocation density in the matrix material. Additionally, analytical results using the shear-lag theory and the Eshelby equivalent inclusion method were compared with experimental results and showed theoretical methods under-predicted the magnitude of strengthening. To account for this under-prediction, Nardone and Prewo [Ref. 11] modified the shear-lag theory to account for matrix-to-fiber load transfer through the fiber tip. An analytical prismatic punching model was later developed by Arsenault and Shi [Ref. 12] to predict the increase in dislocation density and experimentally, Derby and Walker [Ref. 13] used hardness tests to verify strengthening from the dislocations generated by the thermal mismatch.

Recently, Arsenault et al. [Ref. 14] postulated that the observed strength in SiC whisker reinforced aluminum matrix composites can be accounted for by increased

dislocation density and reduced subgrain size in the matrix due to the difference in CTE between the fiber and the matrix. They found using electron microscopy that the dislocation density in the matrix increases with fiber volume fraction and decreases with increasing particle size. Withers et al. [Ref. 15] used a modified Eshelby method in an effort to provide a simple and reliable field model to predict composite properties such as elastic modulus, CTE, residual thermal stress, interfacial bond strength and load transfer in short fiber reinforced metal matrix composites.

Computational approaches have recently gained wide acclaim for their flexibility to include effects such as stress concentration zones at the sharp corners of the reinforcement, and determine the magnitudes of local field quantities, which is essential to the study of thermal residual stresses. Finite element analysis was used by Dutta et al. [Refs. 16, 17] to model the deformation zone in SiC-Al6061 MMC arising from differential thermal contraction. In the latter study it was found that thermal residual stresses can explain the differences between shear-lag models and experimentally observed data and can account for the difference between proportional limit and yield strength in discontinuous fiber composites.

Povirk et al. [Ref. 18] conducted a parametric study of the effects of fiber spacing, volume fraction and fiber aspect ratio. The composite was modeled as a periodic

array of cylindrical unit cells composed of a perfectly aligned thermo-elastic fiber and thermo-plastic matrix. A temperature history was imposed on the cell to simulate the post-fabrication quench. Results indicated that transverse fiber spacing was the most important parameter affecting the distribution and magnitude of the plastic deformation in the matrix, that fiber volume fraction affects the overall level of plastic deformation in the matrix and that fiber aspect ratio has a negligible effect.

#### **B. STRESS-STRAIN BEHAVIOR OF METAL MATRIX COMPOSITES**

Several comprehensive studies have been conducted to examine the dependence of composite stress-strain behavior on material properties such as fiber volume fraction, fiber aspect ratio and fiber spacing. Studies are typically accomplished using two-dimensional finite element analysis, but more accurate account of the presence of adjacent fibers is possible with three-dimensional analysis.

Christman et al. [Ref. 19] conducted a two-dimensional finite element analysis and experimental study of deformation in SiC whisker reinforced aluminum composites under tensile loading. The composite was modeled with various periodic arrays of aligned fibers with cylindrical matrix shells. The matrix was modeled as an elastic viscoplastic solid, subject to isotropic work hardening, and the fiber was modeled as both elastic and perfectly rigid. The numerical

results indicated that large hydrostatic stress states were developed in the matrix during deformation and that plastic deformation occurred first at the fiber tip and then spread throughout the matrix. The results of the parametric study were in qualitative agreement with experimental results, but the model with the more realistic constraints significantly overpredicted elastic modulus, yield strength and tensile strength. The study found that fiber volume fraction was the single most important parameter in determining composite strength, and that the effects of fiber aspect ratio and spacing are strongly dependent on the extent of the constraint imposed on the matrix.

Tvergaard [Refs. 20, 21] used the finite element scheme of Christman [Ref. 19], a staggered (overlapping) fiber arrangement, to account for matrix shearing between adjacent fibers, and a cohesion zone model, to account for fiber debonding. Results indicated that the effect of matrix shearing lowered the magnitude of strength predictions to much closer agreement with experimental data and that fiber debonding occurs first at the fiber corner followed by the fiber top and sidewall surfaces respectively.

Using three-dimensional finite element models, Levy and Papazian [Ref. 22] used aligned and staggered models in longitudinal and transverse tensile loading. The results accurately predicted the elastic modulus and the increase in elastic modulus and work-hardening rate with increasing fiber

volume fraction and fiber aspect ratio. Brockenbrough and Suresh [Ref. 23] used three-dimensional finite element analysis to model various fiber shapes and packing arrangements to study the effect of fiber geometry and distribution on the plastic deformation characteristics of the composite. Results indicated that fiber distribution had a pronounced effect on transverse tensile properties and that the evolution of matrix hydrostatic stresses and plasticity overshadowed all fiber characteristics in longitudinal loading.

To study localized deformation in SiC-Al composites, Arsenault *et al.* [Ref. 24] used two and three-dimensional finite element analysis which accounted for the presence of residual stresses to study clustering effects in the fibers at large fiber volume fractions and monitor the behavior of plastic zones around those whiskers. It was found that plastic deformation is initiated within the region of high fiber concentration and that this clustering results in a reduction of composite flow stress, therefore, the more uniform the fiber distribution the stronger the composite.

### C. STRENGTH DIFFERENTIAL EFFECT

Residual stresses are thought to be the source of the difference in yield strength and flow stress between tension and compression exhibited in metal matrix composites. Arsenault and Taya [Ref. 9] analytically predicted that

differences in yield strength between tension and compression increase with increasing volume fraction. Using the modified Eshelby inclusion method, their results compared well to experimental testing of the short fiber MMC. The authors postulated that this difference was due to a tensile residual stress existing in the matrix.

Dutta [Ref. 16] using finite element analysis, determined that the positive residual shear stresses at the fiber matrix interface, which results from the thermal mismatch, reduce the ability of the matrix to transfer load to the fiber in tension and enhance it in compression. Therefore, the composite compressive strength should be greater than the composite tensile strength. Arsenault and Wu [Ref. 25] experimentally determined the magnitude of this strength differential effect (SDE) and the Bauschinger Effect (BE) of various SiC-Al composites and compared them to the model by Arsenault and Taya [Ref. 9]. Results indicated that the compressive yield strength of whisker and platelet reinforced composites is larger than the tensile yield strength and that the magnitude of the SDE and BE increase with increasing reinforcement volume fraction.

Povirk et al. [Ref. 26] conducted a finite element analysis of the effect of residual stresses on deformation and damage mechanisms in SiC-Al composites. The predicted response with residual stresses in tension and compression was compared to the response without residual stresses. The fiber matrix

interface was also modeled in tension with a specified decohesion parameter to characterize the separation of the interface. Composite cells with a fiber aspect ratio of four and a cell aspect ratio of two and four were compared and results indicated that closer end to end spacing promotes greater flow strength in compression than in tension, and that thermal residual stresses enhance this effect.

#### **D. RESEARCH OBJECTIVES AND OVERVIEW**

Past research efforts have failed to comprehensively examine the effect of thermal residual stresses on composite processing variables and the overall stress-strain response of the whisker reinforced metal-matrix composite. This thesis, and the thesis [Ref. 27] that preceded it, have attempted to take an in-depth look, through finite element analysis, at residual stress effects on the SiC<sub>w</sub>-Al composite. The specific objectives of this thesis include;

1. Study the phenomenology of the matrix and fiber deformation in the composite with and without residual stresses.
2. Study the effect of fiber volume fraction, fiber aspect ratio, and fiber spacing in presence of residual stresses.

Chapter II summarizes the assumptions and methods used in the numerical modeling as well as the material testing procedures. Chapter III contains the results of this investigation, and includes results from the previous

investigation [Ref. 27] for comparison. Chapter IV summarizes the relevant conclusions of the research.

## **II. EXPERIMENTAL APPROACH**

### **A. NUMERICAL MODELING**

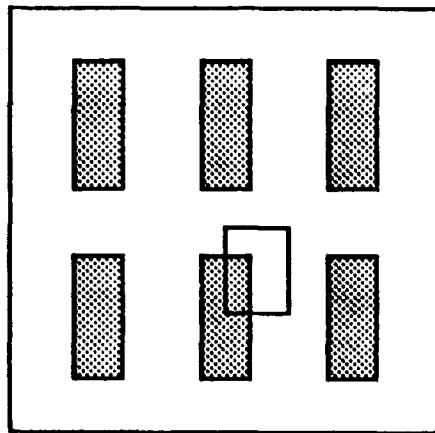
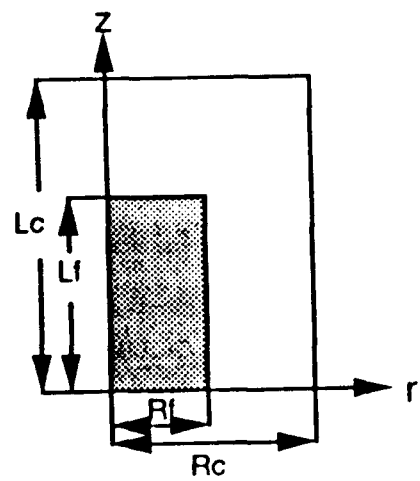
The detailed account of the construction and validation of the numerical modeling employed in this thesis is presented in preceding thesis work by Sims [Ref. 27]. The following is a summary of the methodology and assumptions used in this follow-on study.

#### **1. Finite Element Modeling**

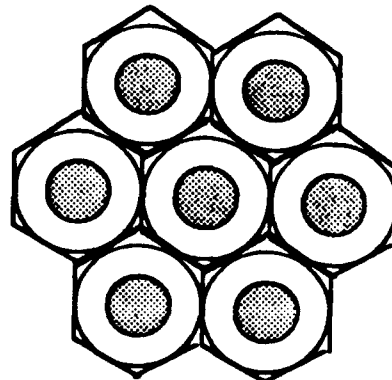
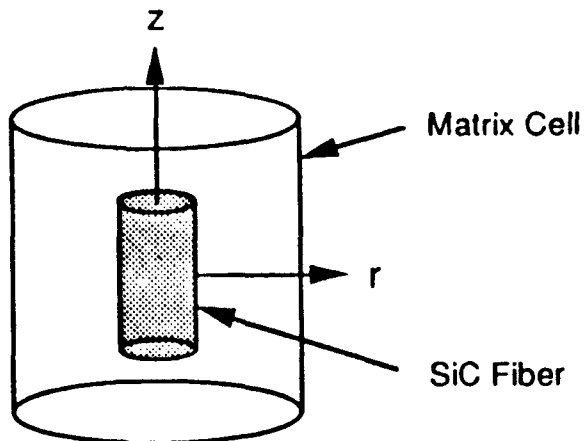
The multipurpose finite-element code, ADINA, was used to predict macroscopic stress-strain behavior, and localized microscopic stress-strain behavior of the metal-matrix composite. Composite and fiber/matrix stress-strain curves and iso-stress/iso-strain contour plots were produced. Two-dimensional axisymmetric analysis was used in conjunction with an Updated-Lagrangian-Jaumann (ULJ) kinematic formulation which uses virtual work to calculate incremental displacements and ultimately elemental stresses. The non-linear response of the material is approximated through an incremental approach based on the Newton-Raphson equations [Ref. 28], that predicts the configuration of the body at the next solution step. The numerical model used two-dimensional iso-parametric elements and second-order Gaussian integration was used for solution accuracy.

The aluminum matrix was characterized by a bilinear stress-strain curve, and was assumed to undergo isotropic work hardening and obey the Von Mises criterion. All material properties were assumed to be constant within the temperature range considered in the study. For aluminum 6061 in the T6 condition, the relevant thermo-mechanical properties are; elastic modulus  $E_{\text{ext.}}=68.3$  GPa and  $E_{\text{corr.}}=69.7$  GPa, work-hardening modulus  $E_h=656$  MPa, yield strength  $\sigma_y=276$  MPa, poisson ratio  $\nu=0.33$ , and CTE= $23.0 \mu\text{K}^{-1}$ ; the SiC fiber values are  $E=450$  GPa,  $\nu=0.2$ , CTE= $4.3 \mu\text{K}^{-1}$ .

Unit cell configuration is similar to the model used by Christman *et al.* [Ref. 19] for an aligned fiber MMC (Figure 1a). The material is assumed to be composed of a periodic array of cylindrical unit cells perfectly aligned with the tensile/compressive axis. Each cell (Figure 1b) is composed of a cylindrical fiber of radius  $R_f$  and length  $L_f$ , surrounded by a matrix shell of radius  $R_c$  and length  $L_c$ . The three-dimensional problem is reduced to two-dimensional by using an axisymmetric modeling approximation which assumes that a structure with rotational symmetry about an axis in the presence of a rotationally symmetric load can be fully described using a two-dimensional model with a unit radian width [Ref. 29]. It can be seen from figure 1b, that the axisymmetric model is an appropriate analog to the three-dimensional array of hexagonal unit cells [Ref. 19].



(a)



(b)

**Figure 1.** Material Representation: Diagram Showing (a) the Aligned Fiber Arrangement and (b) a Depiction of the Fiber Imbedded in the Matrix Shell.

## **2. Boundary Conditions**

The ADINA code dictates displacement-based boundary conditions be specified along with the master degrees of freedom for the entire finite-element model. A cylindrical coordinate system was used with displacements  $u_z$  and  $u_r$  corresponding to the z and r axes, respectively. For the aligned fiber model, the boundary conditions required for symmetry are  $u_r=0$  along  $z=0$  and  $u_z=0$  along  $r=0$ . The boundary conditions required for constraint by adjacent unit cells are that  $u_z$  on  $z=L_c$  and  $u_r$  on  $r=R_c$  be constrained to preserve the right circular cylindrical shape of the unit cell, therefore the top and lateral surfaces of the cell remain planer throughout the quench and the loading process.

Perfect bonding is assumed along the fiber-matrix interface. This is accomplished in ADINA by specifying that the fiber and matrix elements adjacent to the interface share the same boundary nodes, thereby precluding the possibility of separation during the loading sequence.

## **3. Applied loading**

The loading scheme used in the numerical modeling combines thermal and displacement loads in a sequence designed to approximate those experienced by the composite during fabrication and subsequent compressive and tensile loading. The post-fabrication quench is accomplished by subjecting all nodes in the unit cell to a  $505^{\circ}\text{C}$  temperature drop from the

solutionizing temperature ( $530^{\circ}\text{C}$ ) to room temperature ( $25^{\circ}\text{C}$ ) in a single solution step, which eliminates any quench rate or bulk thermal effects. The resulting nodal displacements from the quench are stored in a restart file to be used as the initial nodal displacements during the tensile and compressive analysis.

Tensile and compressive loading of the model is accomplished by applying an axial displacement of  $\Delta L_c = (e^{\epsilon} \pm 1) L_c$  where  $\epsilon$  is the applied true strain,  $L_c$  is post-quench cell length, and  $\Delta L_c$  is applied to the top surface of the unit cell. The composite stress-strain curves are constructed by applying a  $\Delta L_c$ , corresponding to a selected value of  $\epsilon$  to the model. The average axial stress was calculated using a volume average approach as follows:  $\sigma_{zzc} = (1/V_c) \int \sigma_{zzf} dV_f + (1/V_c) \int \sigma_{zzm} dV_m$  where subscripts c, f, and m correspond to composite, fiber, and matrix respectively. In this equation each  $\sigma_{zz}$  represents an average of the four appropriate Gaussian integration points within each element of the cell. The average elemental stresses are then multiplied by their corresponding elemental volumes and summed over the entire volume of the composite.

#### **4. Grid Independence**

A Full-Newton iterative scheme was selected for use in this study, the out-of-balance energy, with a tolerance set at  $10^{-6}$ , was determined to be the basis for convergence. The mesh for each model was uniformly refined until two successive

values of  $\sigma_{zz}$  at  $\epsilon_c=0$  (residual axial stress in the as-quenched condition) gave results that agreed to within 10%. This parameter was found to be the most sensitive to changes in mesh size and therefore was determined to be the most suitable to establish grid independence.

### **5. Model Implementation**

The numerical models discussed above were modified for the particular variable whose effect was being evaluated. For the models used to study fiber volume fraction effects, the fiber and the cell aspect ratios were both fixed at 6 and numerical results were carried out for volume fractions of 10%, 20%, and 30%. For the fiber aspect ratio study, the fiber volume fraction was held at 30%; the fiber aspect and cell aspect ratios were set equal to one another and numerical results were carried out for values of 1, 3, 6, and 10. For the fiber spacing study, the fiber volume fraction was again held at 30%; the fiber aspect ratio was held at 5, and numerical results were carried out for a cell aspect ratio of 3, 6, and 10. The models used to approximate experimental data were assigned values of 3 for both fiber cell and fiber aspect ratios and numerical results were carried out for volume fractions of 20% and 30%.

Composite stress-strain curves and appropriate fiber loading curves were produced in tensile and compressive loading, with and without residual stresses. Iso-stress

contour plots of Von Mises effective stress, axial stress, and hydrostatic stress in addition to iso-strain contour plots of cumulative effective plastic strain were generated in tension and compression, with and without residual stresses. The aforementioned results were compared and contrasted to determine the effects of residual stresses on the metal-matrix composites

#### **B. MATERIAL TESTING**

Two different types of SiC whisker reinforced composite material were tested in tensile and compressive loading to extract mechanical properties for the use in the numerical models and to serve as a comparison to assess the accuracy of the numerical predictions. The composites were procured from Advanced Composite Materials Corporation (ACMC), Greer, SC, and were produced using powder metallurgy (P/M) techniques. Test samples were made by the manufacturer from a 20 vol.% SiC/Al 6061 MMC with a extrusion ratio of 11:1 and a 30 vol.% SiC/Al6061 MMC with an extrusion ratio of 6.5:1, and both materials were heat treated to the T6 condition. Unreinforced Al 6061-T6 testing samples were machined from plate stock.

All specimens were cut from extruded stock such that the longitudinal axis of the sample was aligned with the extrusion direction. Samples were mounted in a screw-driven Instron machine and tested at a rate of 0.127 mm/min. Tensile specimens with 1.0" gage lengths were tested with clip-on

extensometers to record engineering strain values. Compression samples with 1.0" gage lengths and length to thickness ratios of approximately 2.5, to avoid buckling, were tested without clip-on extensometers. A more accurate means of testing materials, to be compared in compression and tension, would include using identical test specimens with extensometers in a testing rig designed for both tension and compression.

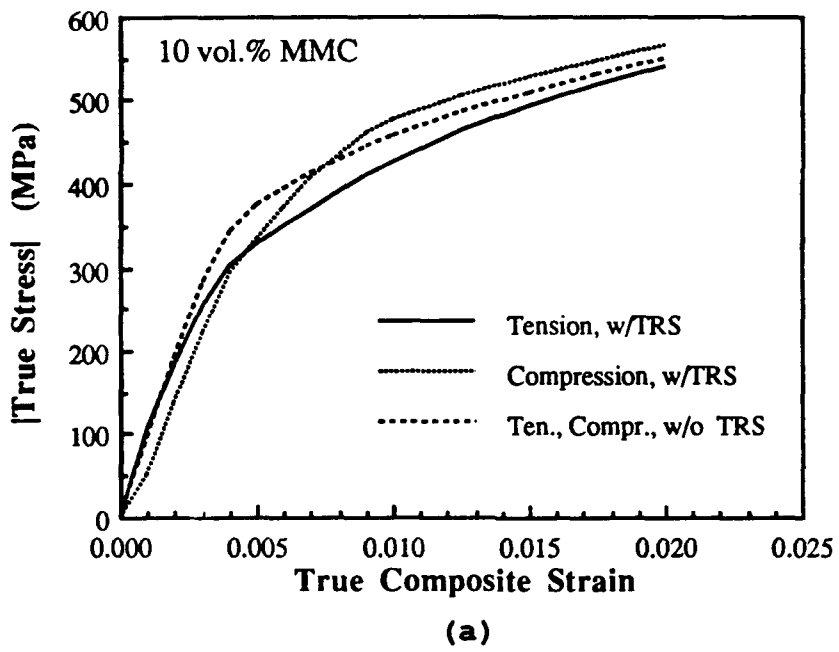
Scanning electron microscopy was used to obtain micrographs of the 20 and 30 vol.% MMC, to determine average values of the fiber aspect ratio and cell aspect ratio, and to serve as a microstructural comparison for the numerical modeling.

### **III. RESULTS**

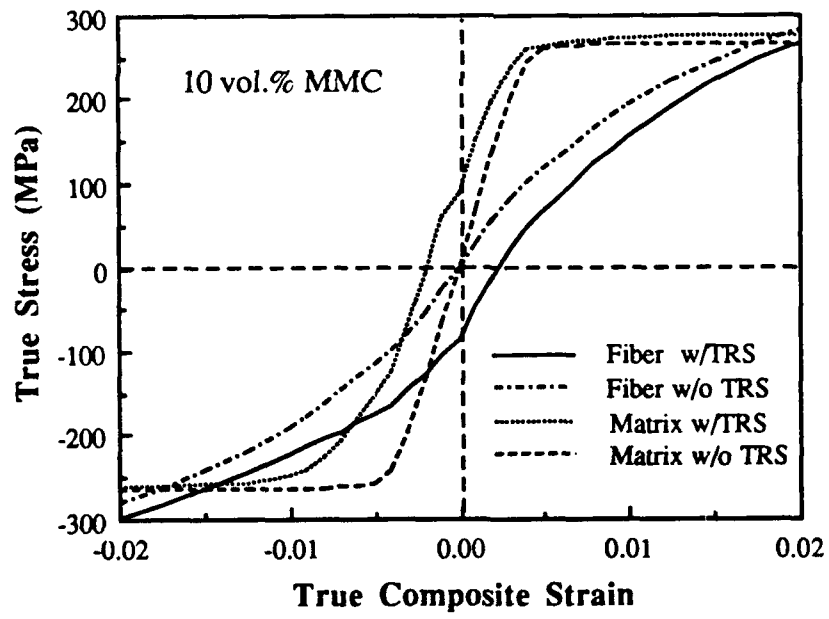
#### **A. EFFECTS OF THERMAL RESIDUAL STRESSES: A PHENOMENOLOGICAL STUDY**

##### **1. Constitutive Composite Response**

The primary aim of this study has been to assess the role of thermal residual stresses (TRS) on the stress-strain behavior of the metal-matrix composite. The results contained in this section will describe the behavior for a composite with 10 vol.% SiC whiskers with a fiber aspect ratio of 6 and a composite cell aspect ratio of 6. Figure 2a compares the aligned-fiber model with and without thermal residual stresses (TRS) in both uni-axial tensile and uni-axial compressive loading. The numerical model predicts a Young's modulus ( $E$ ) in tension of 76.2 GPa, a modulus in compression of 88.8 GPa, and a modulus of 94.8 GPa without TRS. The model predicts a yield strength (YS) of 368 MPa in tension, 385 MPa in compression, and 400 MPa without TRS. Most importantly, the model shows a significant decrease in flow stress in tension and a corresponding increase in flow stress in compression when compared to the model without TRS. Additionally, Figure 2b shows that in both loading cases with TRS present, the proportional limit is smaller and the work-hardening rate is slightly higher when compared to loading without TRS.



(a)



(b)

**Figure 2.** Residual Stress Effects: Effects of Thermal Residual Stresses (TRS) in Tension and Compression. (a) Composite Stress-Strain Behavior and (b) Fiber and Matrix Stress-Strain Behavior.

When TRS are not present, the constitutive stress-strain behavior of the composite is essentially the same in both tension and compression. Figure 2b shows the matrix, after post-fabrication quench, is initially at an average tensile stress ( $\sigma_{zz,V_0}$ ) of 88 MPa; therefore the start of macroscopic matrix plastic deformation begins at a smaller strain level in tensile loading than in compressive loading, where the matrix must undergo relaxation from its tensile state prior to a build-up in compression and subsequent macroscopic plastic deformation of the matrix. This may explain the smaller Young's modulus observed in compressive loading with TRS present.

It must be noted that an initial transient occurs, predicting an initial composite modulus higher than expected in tensile loading and lower than expected in compressive loading. This could be explained by the tensile residual stress imposed on the matrix by the post-fabrication quench. In tension, this residual stress would increase and allow for immediate load transfer to the fiber, which will undergo a stress reversal from its initial compressive residual stress state. In compression, this initial tensile residual stress in the matrix must undergo a stress relaxation and reversal prior to additional compressive load transfer on the fiber. Further study is required in this area at very small strains to substantiate the preceding explanation.

When comparing Figure 2a and Figure 2b, the composite 0.2% offset yield stress in tensile loading occurs well after the matrix has reached its apparent yield point on the matrix stress-strain curve, both in the presence and absence of TRS. In compression, the 0.2% offset yield stress occurs prior to the matrix reaching its apparent yield point on the matrix stress-strain curve. It should be noted from Figure 1, that in this region the composite stress-strain curve in compressive loading crosses both the tensile loading curve and the curve without TRS, while there is no indication of this trend in the fiber and matrix curves of Figure 2b.

Thermal residual stresses induce a positive residual shear stress at the fiber matrix interface. This residual shear stress is added to any applied shear stress from an applied load, negative in tensile loading and positive in compressive loading. The absolute value of this quantity is indicative of the amount of matrix-to-fiber load transfer in the composite in uni-axial loading. In the case of two equal but opposite loadings, it is clear that the composite under compression should exhibit the largest load transfer, and subsequently the largest strength.

Figure 2a illustrates that the flow stress of the composite is greater in compression than in tension throughout the plastic region of the composite response when residual stresses are present. This suggests that either matrix-to-fiber load transfer or matrix work-hardening plays a

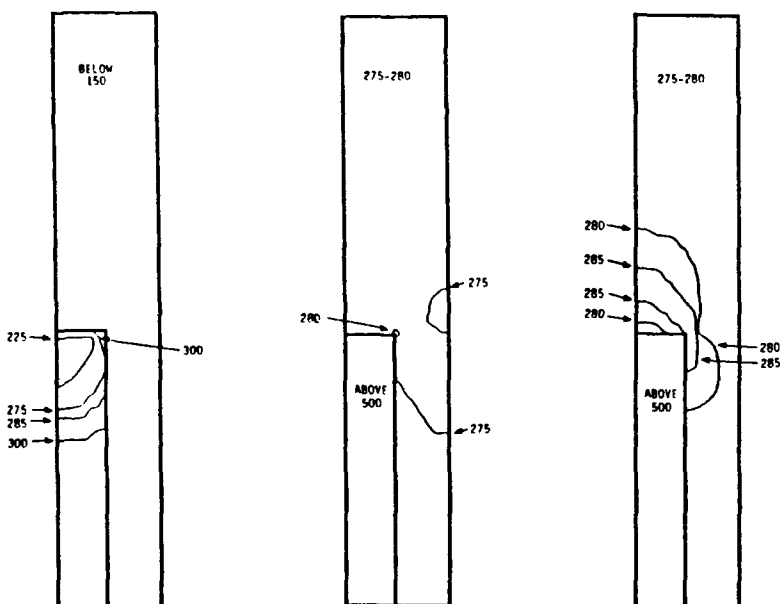
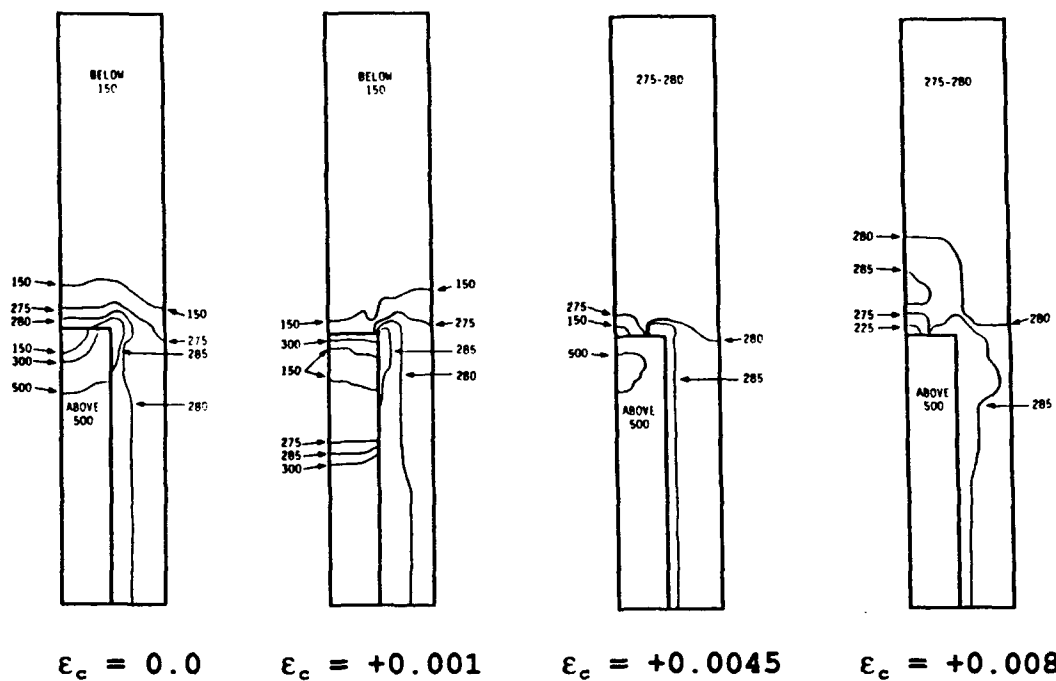
significant role in the strength difference of MMCs in compression and tension. From Figure 2b it is apparent that load transfer may play the important role in the stress-strain behavior of the composite. Under tensile loading, the fiber carries less load and the matrix carries a greater percentage of the load than the MMC without TRS. Under compressive loading, this is reversed, the fiber carries more load and the matrix carries less load than the MMC without TRS.

The work-hardening rate of the matrix is higher in both tension and compression with TRS present. The composite work-hardening rate is slightly greater in tension and nearly the same in compression as the MMC without TRS present, which is probably due to the initiation of macroscopic plastic deformation in the matrix at a smaller strain in tension than in compression.

## **2. Plastic Zone Initiation and Growth: Von Mises Effective Stress**

Figure 3 shows one quadrant of the unit cell of a 10 vol.% whisker reinforced composite model with a fiber aspect ratio and composite cell aspect ratio of six ( $A_f=6, A_c=6$ ), at selected levels of uni-axial tensile strain with and without TRS. Iso-stress contours of Von Mises effective stress are plotted within the model cells to show regions of the matrix which are plastically deforming. The contour plot of residual effective stress ( $\epsilon_c=0.0$ ) reveals that a plastically deformed zone ( $\sigma_{eff}>275$  MPa) exists in the matrix along the entire

**with residual stress**



**without residual stress**

**Figure 3.** Plastic Zone Development-Von Mises Effective Stress in Tension: Contours of Effective Stress for a 10 vol.% MMC ( $A_f=A_c=6$ ) With and Without Residual Stress.

fiber-matrix interface with the highest stress occurring in the vicinity of the fiber corner. The contour plot also indicates plastic deformation has occurred throughout the matrix region adjacent to the lateral fiber sidewall. This stress is highest at the lateral fiber-matrix interface and decreases towards the cell boundary. The effective stress levels in the elastic fiber are characterized by a large stress zone in excess of 500 MPa in the middle of the fiber, and a relatively low effective stress near the tip of the fiber. Physically, the 10 vol.% MMC has a large volume of matrix material surrounding the fiber. Upon quenching, the matrix contracts around the fiber resulting in a high residual compressive stress in the fiber and a tensile residual stress in the matrix surrounding the fiber. Additionally, as the matrix tries to relieve the residual stresses, it will deform plastically at the vicinity of the interface.

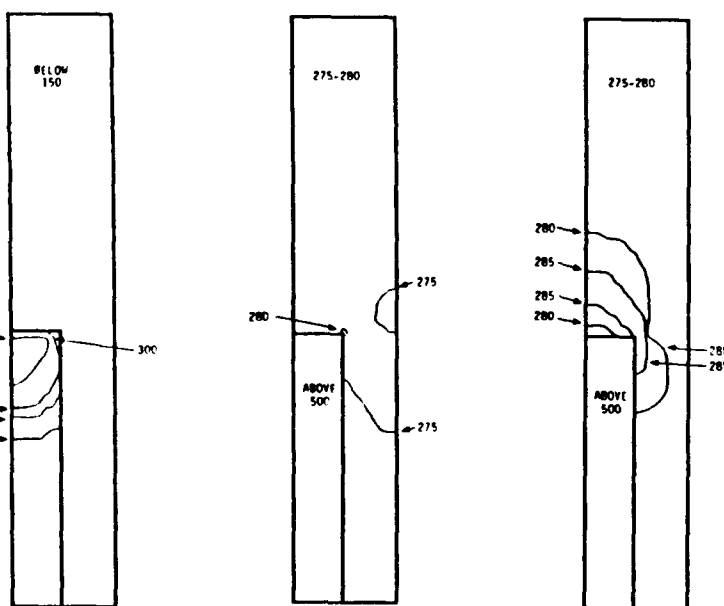
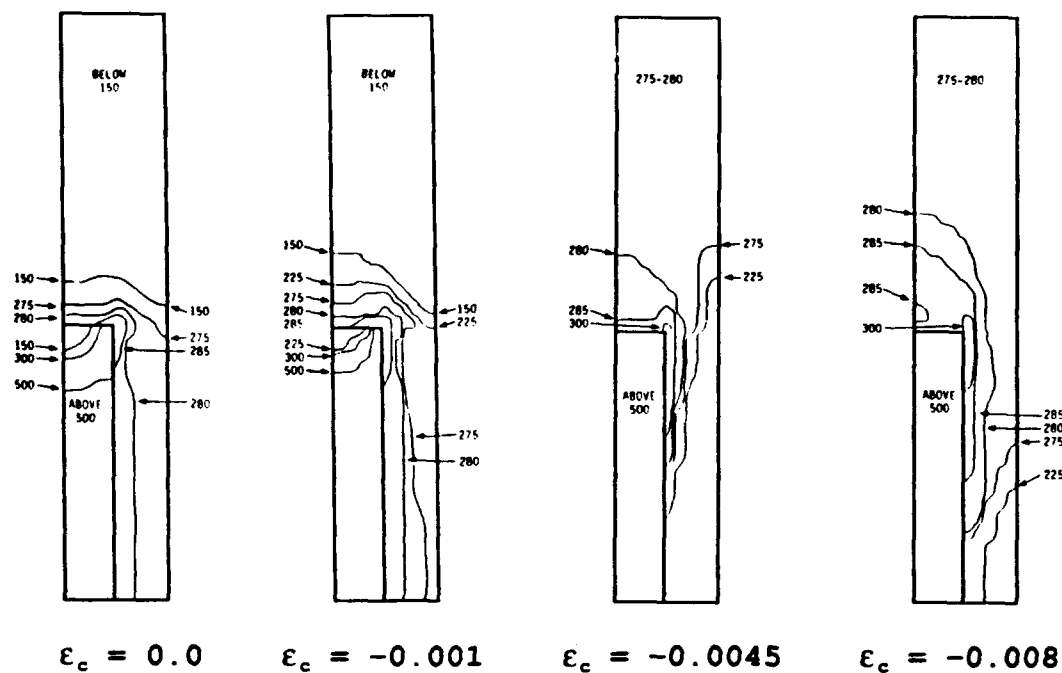
At a small tensile strain ( $\epsilon_c=+0.001$ ), the plastic zone along the lateral surface of the interface begins to expand in the radial direction. The matrix region adjacent to the top of the fiber experiences a stress relaxation as load is transferred from the matrix to the fiber across the fiber-tip and end surface. This effect is evident in the growth of a high stress region at the tip of the fiber, indicative of the fiber bearing a greater portion of the applied load at the fiber-tip. At moderate strains ( $\epsilon_c=+0.0045$ ), the effective Von Mises stress in the matrix increases next to the fiber-tip, as

well as the lateral interface, indicating growth in the plastic zone size which, at further strain, advances to cover the entire matrix.

Figure 4 shows the same quadrant of the 10 vol.% MMC detailed above, with iso-stress contours of Von Mises effective stress plotted within the MMC cell model at selected levels of uni-axial compression with and without TRS. The MMC without TRS exhibits nearly identical behavior in both tension and compression. Although the loading is in the opposite direction, the effective stress contour plots are nearly identical.

At a small compressive strain ( $\epsilon_c = -0.001$ ), the behavior of the 10 vol.% MMC is different from that under tensile loading, the effective Von Mises stress next to the lateral fiber-matrix interface decreases, probably suggesting an increase in the matrix-to-fiber load transfer across the side wall of the fiber. The plastically deformed matrix region adjacent to the end of the fiber begins to expand towards the top of the cell. Contrary to the tensile case, TRS in compressive loading enhance load transfer across the lateral fiber-matrix interface, but do not result in enhanced load transfer at the fiber-tip. At a moderate compressive strain ( $\epsilon_c = -0.0045$ ), the lateral matrix adjacent to the fiber sidewall continues its relaxation. The effective stress in this region near the middle of the cell is well beneath the yield stress of the matrix ( $\sigma_{eff} < 275$  MPa), and is indicative of

**with residual stress**



**without residual stress**

**Figure 4.** Plastic Zone Development-Von Mises Effective Stress in Compression: Contours of Effective Stress for a 10 vol.% MMC ( $A_f=A_c=6$ ) With and Without Residual Stress.

significant matrix-to-fiber load transfer through the sidewall. The matrix area above the fiber-tip has entirely plastically deformed, and the very high stress level in the matrix region of the fiber corner has spread along the interface. At a higher compressive strain ( $\epsilon_c = -0.008$ ), the effective stress contour plot reveals that plastic deformation in the matrix has increased next to the lateral fiber-matrix interface and continued next to the fiber-tip to cover the entire composite matrix.

### **3. Cumulative Effective Plastic Strain**

Figure 5 shows one quadrant of the 10 vol.% MMC with the same fiber aspect ratio ( $A_f=6$ ) and composite cell aspect ratio ( $A_c=6$ ) as before. Iso-strain contour lines of cumulative plastic strain are plotted within the model cells at equal strain values ( $\epsilon_c = \pm 0.010$ ) in tension with TRS, compression with TRS, and compression/tension without TRS. The contour plots exhibit higher levels of plastic strain in the matrix along the lateral fiber-matrix interface in tension and higher levels of plastic strain in the matrix region above the fiber-tip in compression. Both models exhibit larger plastic strain, and therefore greater work-hardening when compared to the model without TRS present. It is apparent that TRS impede matrix work-hardening by enhancing matrix-to-fiber load transfer across the fiber-tip in tension and across the lateral fiber-matrix interface, which relaxes the effective

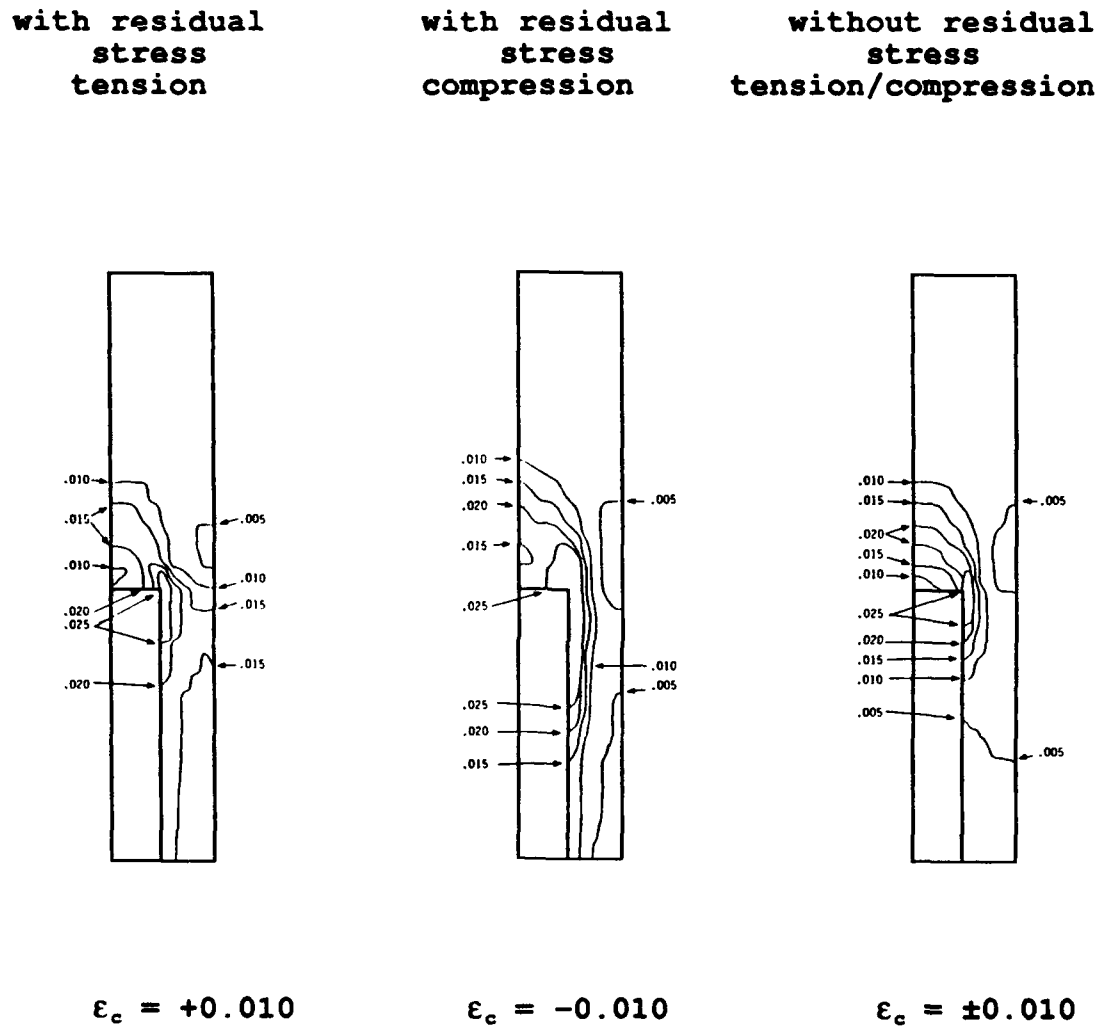


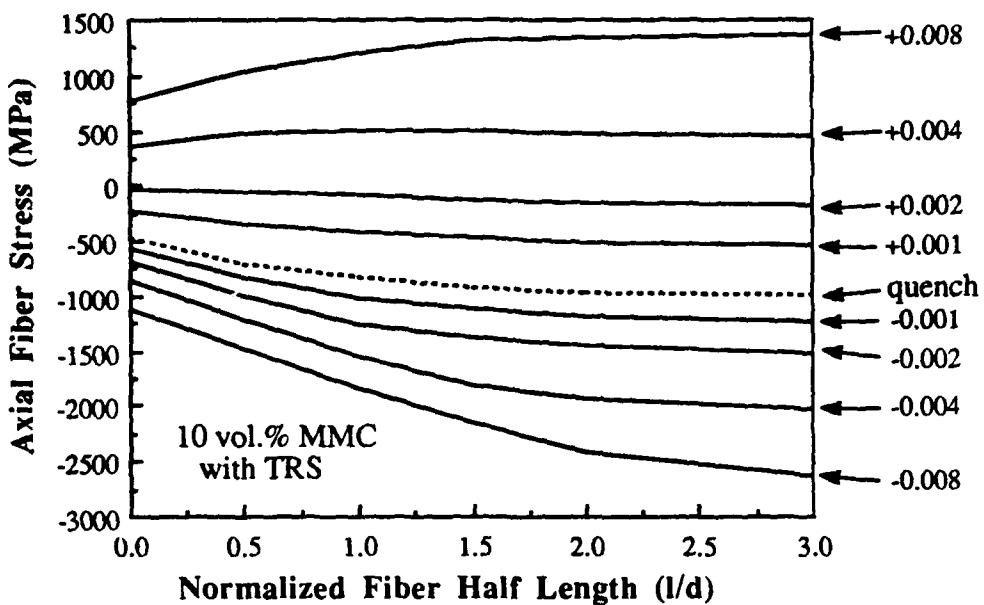
**Figure 5.** Cumulative Effective Plastic Strain: Effective Plastic Strain for a 10 vol.% MMC with  $A_f=A_c=6$  at an Equivalent Value of Strain ( $\epsilon_c=0.010$ ) in Tension With Residual Stresses, Compression With Residual Stresses, and Tension/Compression Without Residual Stresses.

stresses in the adjacent matrix and therefore slows the accumulation of plastic strain.

#### **4. Fiber Loading in Tension and Compression**

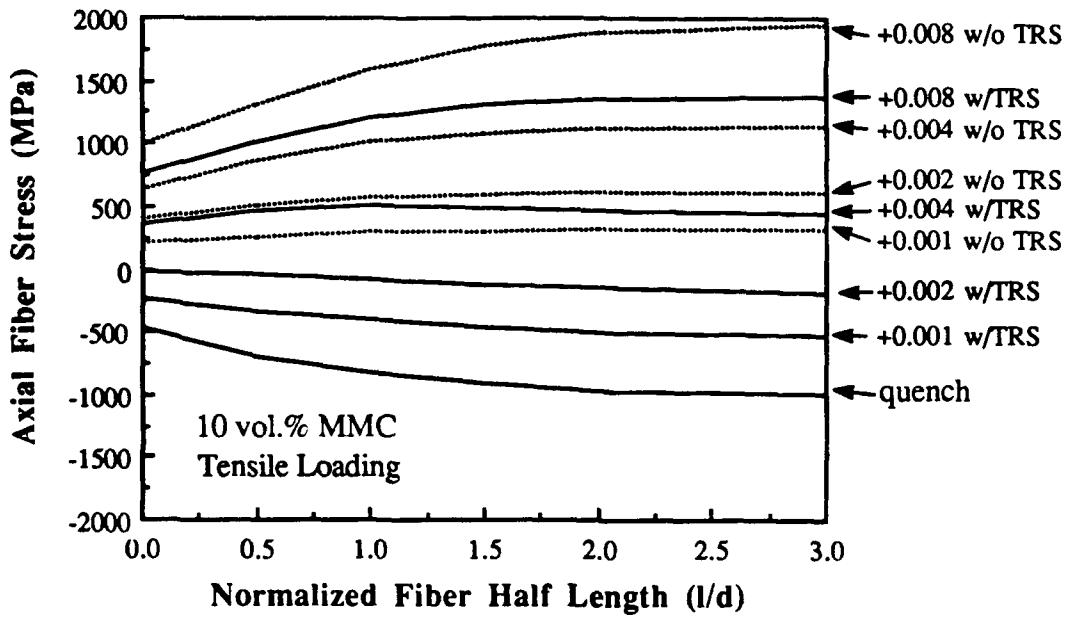
Figure 6 illustrates the axial stress along half of the fiber in the 10 vol.% MMC ( $A_f=6, A_c=6$ ) at selected increments of tension and compression. The residual axial fiber stress ( $\sigma_{zz}$ ) in the as-quenched state, ranges from -450 MPa at the fiber-tip to -1000 MPa at the middle of the fiber. In tensile loading, the axial stress along the fiber relaxes from its residual compressive state, and subsequently begins loading in tension. In compressive loading, the fiber exhibits further compressive loading, but at a lower initial loading rate than in tension. Notably, the magnitude of the tensile stress carried by the fiber is significantly lower than the magnitude of compressive stress carried by the fiber at equal values of tensile and compressive strain. Additionally, the incremental increase in the magnitude of the stress supported by the fiber is much larger in tension than in compression.

Figure 7a, a comparison of axial stress along the fiber half length with and without TRS, shows that the fiber with TRS supports smaller axial tensile stress at equivalent values of composite strain ( $\epsilon_c$ ). Conversely, in compressive loading (Figure 7b), the fiber with TRS supports a much greater axial compressive stress load than in the absence of TRS.

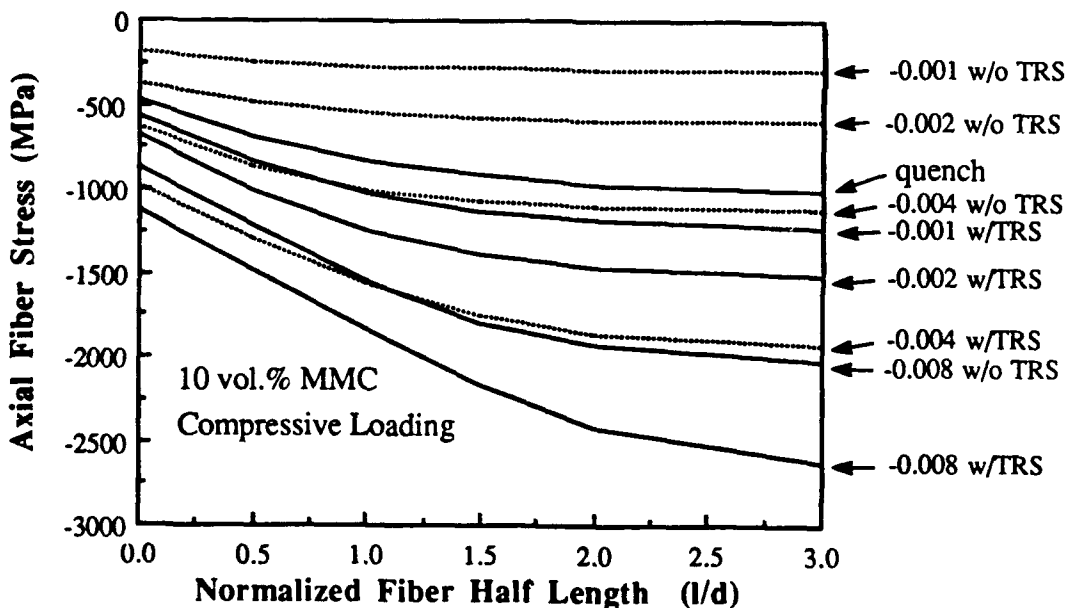


**Figure 6.** Axial Fiber Stress With Residual Stresses Present: Axial Stress Carried by the Fiber ( $A_f = A_c = 6$ ), Indicated Levels of Composite Strain at Right, Fiber Tip at 0.0, Fiber Middle at 3.0.

In Figure 6, the magnitude of the fiber-tip axial stress is graphed for selected strain regimes. In tensile loading, the stress carried by the fiber-tip is greater over all strain regimes with TRS than without. The opposite is true in compressive loading, where the fiber-tip stress is less with TRS. This comparison suggests that TRS cause the MMC to have a larger load transfer rate across the tip of the fiber in tension and a smaller load transfer rate across the fiber-tip in compression.



(a)



(b)

**Figure 7.** Axial Fiber Stress With and Without Residual Stresses: Axial Stress Carried by the Fiber in (a) Tension and in (b) Compression.

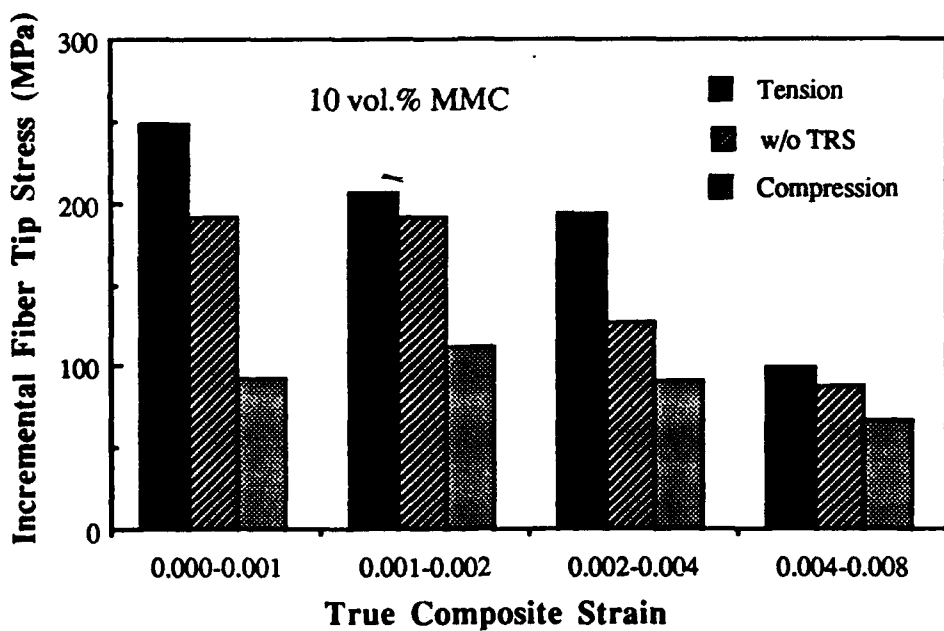
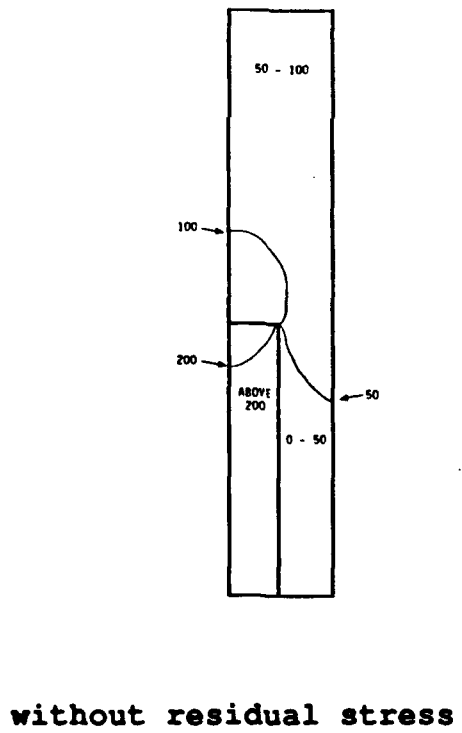
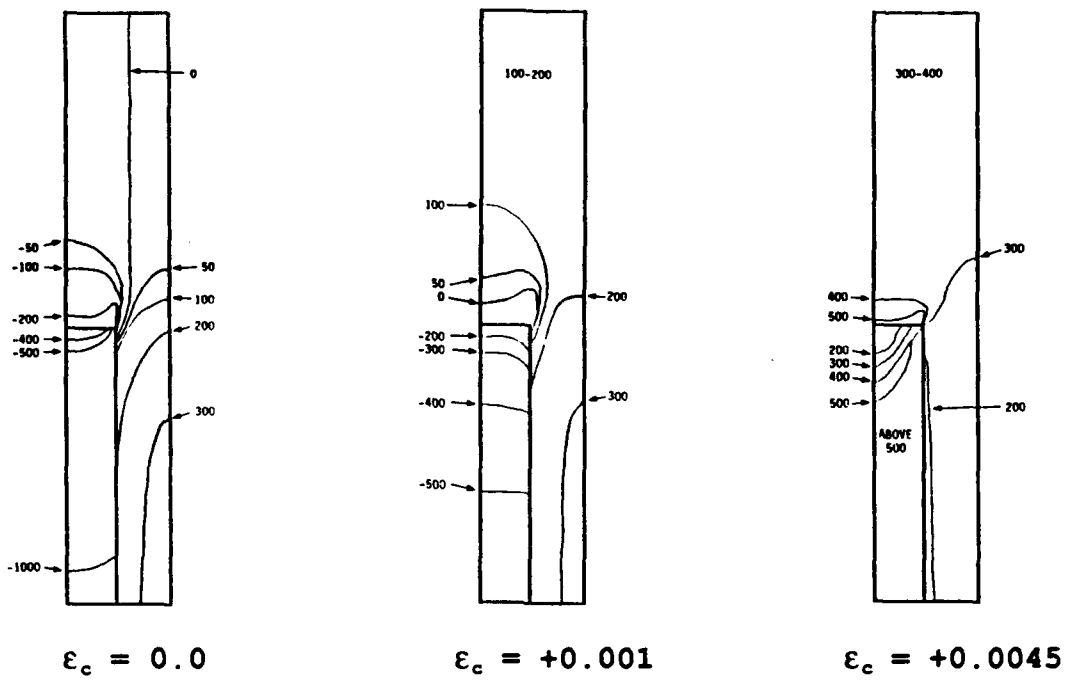


**Figure 8.** Incremental Fiber Tip Stresses With and Without Residual Stresses: Incremental Fiber Tip Stress ( $\sigma_{zz(fiber-tip)}/\Delta\epsilon_c$ ) for Indicated Stress Regimes in Tension and Compression.

### 5. Axial Stresses in the Composite

Figure 9 shows a quarter cell of the 10 vol.% MMC at selected values of uni-axial tension with and without TRS. The iso-stress contours of axial residual stresses at  $\epsilon_c=0.0$  exhibit a fiber under purely compressive stress ( $-1000 < \sigma_{zz} < -300$  MPa). The matrix region is compressive directly above the fiber, and tensile next to the lateral fiber-matrix interface. The models without TRS in tension and compression, with appropriate sign changes, exhibited essentially the same iso- $\sigma_{zz}$  contour plots.

**with residual stress**



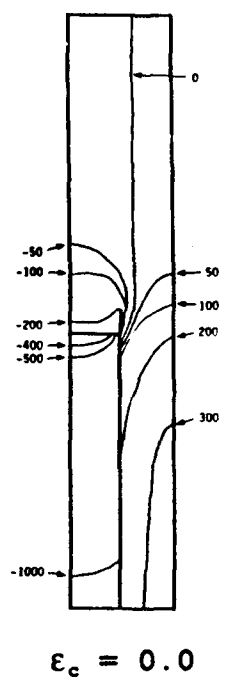
**without residual stress**

**Figure 9.** Axial Stress in Tension: Contours of Axial Stress for a 10 vol.% MMC ( $A_f=A_c=6$ ) With and Without Residual Stress.

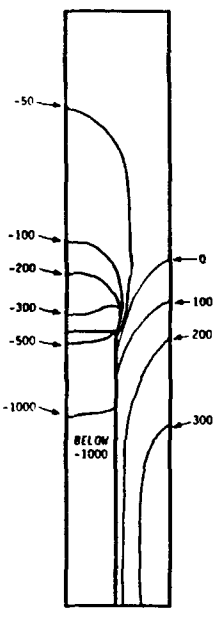
At a small tensile strain ( $\epsilon_c=+0.001$ ), the fiber, still in compression, undergoes a substantial stress relaxation most notably at the middle. Concurrently, the matrix experiences a large stress increase ( $\sigma_{zzm}=+100$  MPa) in the region above the fiber-tip, and only a slight stress increase in the lateral matrix-fiber interface region. This large change in the stress carried by the middle of the fiber, and the coinciding small change in stress carried by the matrix region adjacent to the fiber-matrix interface may indicate that the predominant means of matrix-to-fiber load transfer in the MMC is through the fiber sidewall. At a larger tensile strain ( $\epsilon_c=+0.0045$ ), the stress in the matrix above the fiber-tip has continued to increase, but the stress carried by the matrix adjacent to the lateral fiber-matrix interface has actually decreased. Another possible reason for this decrease in stress besides matrix-to-fiber load transfer is the outer cell wall boundary condition forcing the lateral matrix adjacent to the fiber to relax as the cell wall moves in response to controlling Poisson ratio demands in the upper matrix or the symmetry requirements from the adjacent cell. When compared with the MMC in tension without TRS, there was some evidence of a smaller net increase in axial stress in the matrix region above the fiber-tip with TRS, suggesting greater load transfer through the fiber-tip when residual stresses are present.

Figure 10 shows the same quarter cell of the MMC in uni-axial compression with and without TRS. The iso-stress

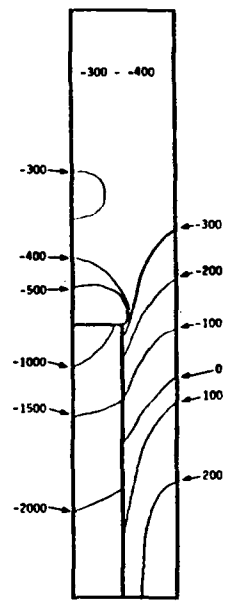
**with residual stress**



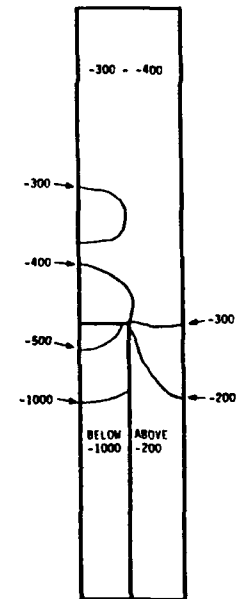
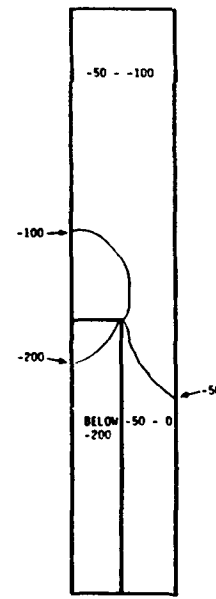
$\epsilon_c = 0.0$



$\epsilon_c = -0.001$



$\epsilon_c = -0.0045$



**without residual stress**

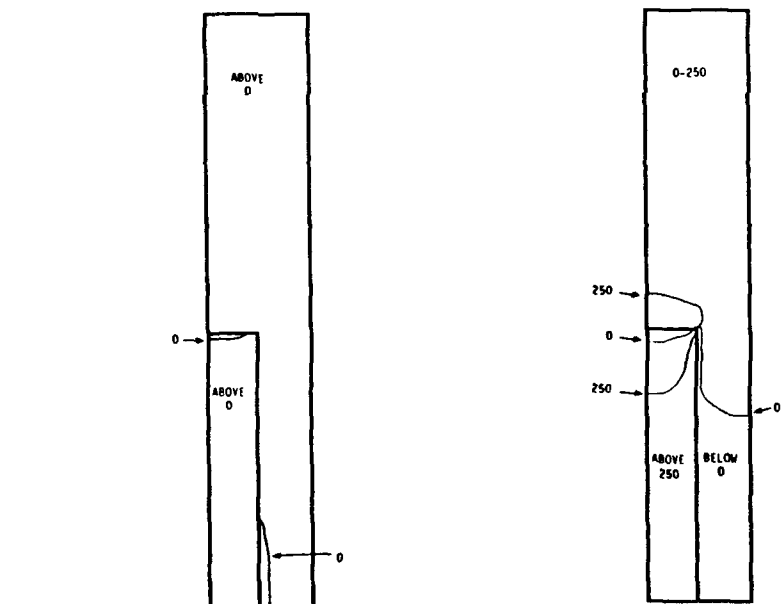
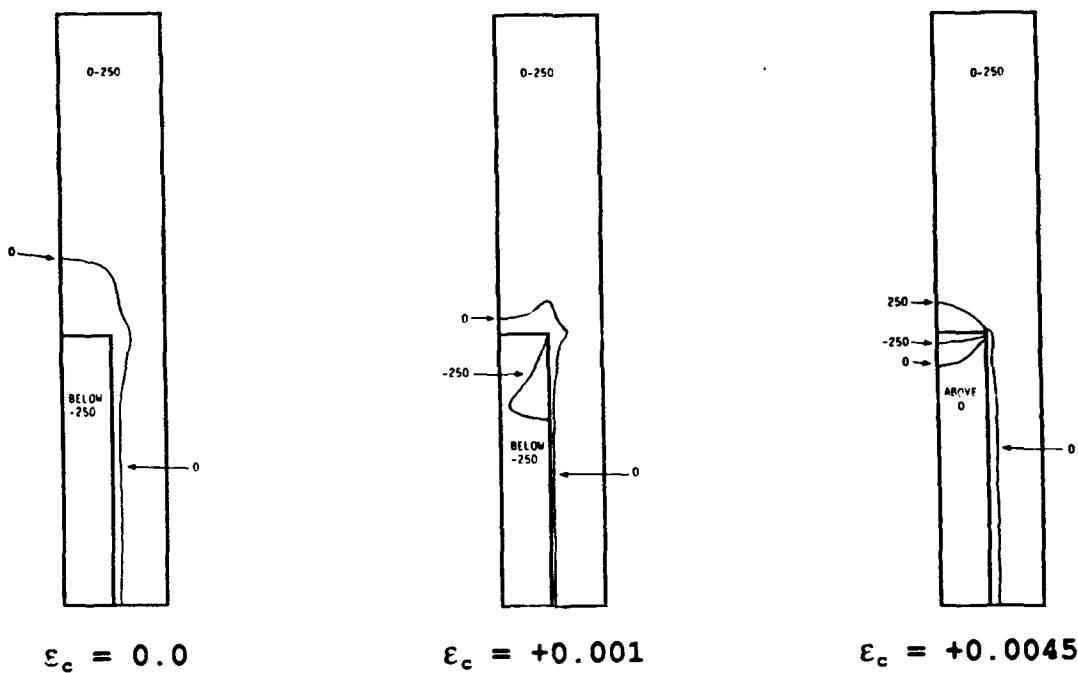
**Figure 10.** Axial Stress in Compression: Contours of Axial Stress for a 10 vol.% MMC ( $A_f=A_c=6$ ) With and Without Residual Stress.

contours of axial stress exhibit that at a small compressive strain ( $\epsilon_c = -0.001$ ), the middle of the fiber exhibits increased compressive stress relative to the quenched state. The matrix region above the fiber end shows an increase in the compressive stress relative to the as quenched state, while the lateral matrix area remains essentially at the same stress level as after the quench. At a larger compressive strain ( $\epsilon_c = -0.0045$ ), the fiber and the matrix above the fiber exhibit continued increase in the compressive stress, while the matrix next to the lateral fiber-matrix interface exhibits a continued reduction in the tensile stress without the expected transformation to a compressive stress state. The lack of significant tensile stress relaxation in the lateral matrix area suggests either effective matrix-to-fiber load transfer across the fiber sidewall or the outer cell wall boundary condition imposing constraints on the lateral matrix as discussed previously. When compared to the MMC in compression without TRS, there is some evidence of a larger net decrease in axial stress in the matrix region above the fiber-tip when residual stresses are present, indicating less matrix-to-fiber load transfer across the fiber-tip when TRS are present.

## **6. Hydrostatic Stresses in the Composite**

Figure 11 shows a quarter cell of the 10 vol.% MMC at selected values of uni-axial tension with and without TRS. The iso-stress contours of hydrostatic residual stresses ( $\epsilon_c = 0.0$ )

**with residual stress**



**without residual stress**

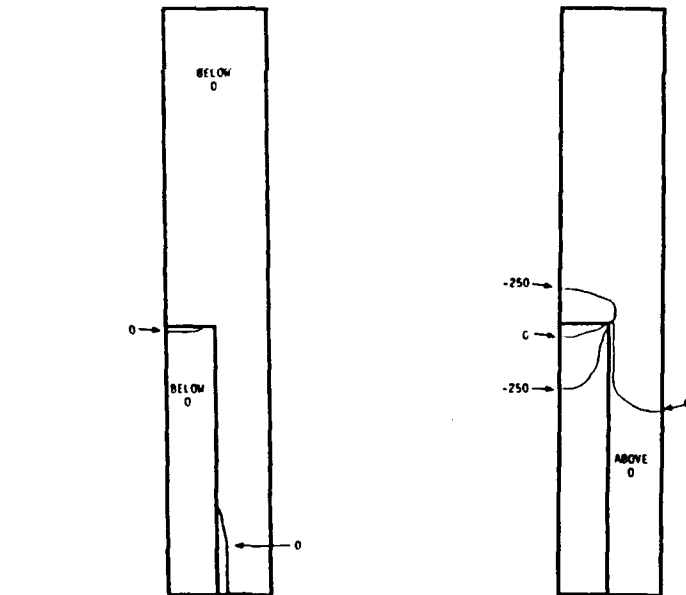
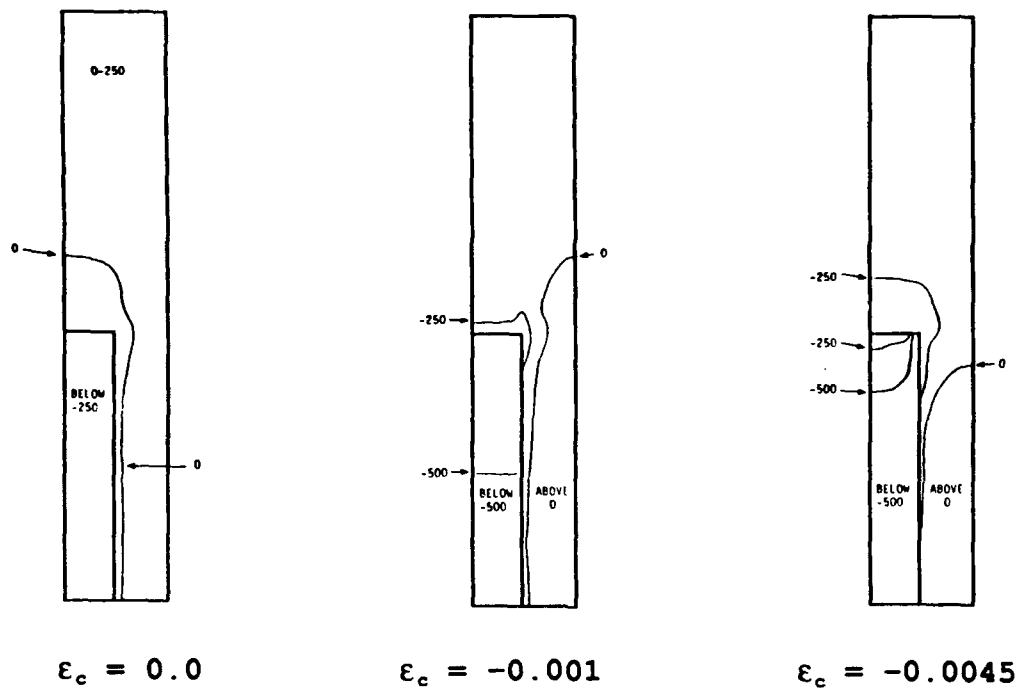
**Figure 11.** Hydrostatic Stress in Tension: Contours of Hydrostatic Stress for a 10 vol.% MMC ( $A_f=A_c=6$ ) With and Without Residual Stress.

exhibit a large compressive hydrostatic stress region ( $-250 < \sigma_{xy} < 0.0$  MPa) in the matrix above the fiber-tip, that continues to the lateral matrix region at the fiber-matrix interface, with the remainder of the matrix in tensile hydrostatic stress ( $0.0 < \sigma_{xy} < 250$  MPa).

Under tensile strain ( $\epsilon_c = +0.001 \& +0.0045$ ), the compressive matrix region above the fiber-tip contracts and becomes tensile while the matrix region adjacent to the lateral fiber-matrix interface remains in compressive hydrostatic stress, suggesting that crack nucleation in the MMC will occur first at the fiber-tip. When compared to the MMC with TRS, the MMC without TRS exhibits tensile hydrostatic stresses throughout most of the matrix region. This suggests that residual stresses may actually inhibit the onset of crack nucleation at both the fiber-tip and lateral fiber-matrix interface.

Figure 12 shows the same quarter cell of the MMC in uni-axial compression with and without TRS. The iso-stress contours of hydrostatic stress exhibit that in compressive strain ( $\epsilon_c = -0.001 \& -0.0045$ ), the matrix region in hydrostatic compression adjacent to the lateral fiber-matrix interface, next to the middle of the fiber, contracts and becomes tensile. This suggests crack nucleation via debonding of the interface is likely to occur at the lateral fiber-matrix interface close to the middle of the fiber in compressive loading. When compared with the model with TRS, the MMC

**with residual stress**



**without residual stress**

**Figure 12.** Hydrostatic Stress in Compression: Contours of Hydrostatic Stress for a 10 vol.% MMC ( $A_f=A_c=6$ ) in Compression With and Without Residual Stress.

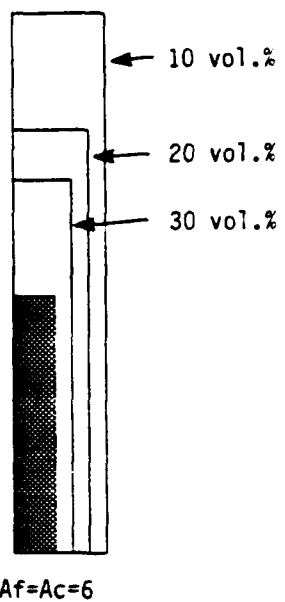
without TRS exhibits a hydrostatic tensile stress zone along..  
the entire lateral fiber-matrix interface, suggesting TRS may  
inhibit debonding at fiber-matrix interface.

## B. PARAMETRIC STUDY

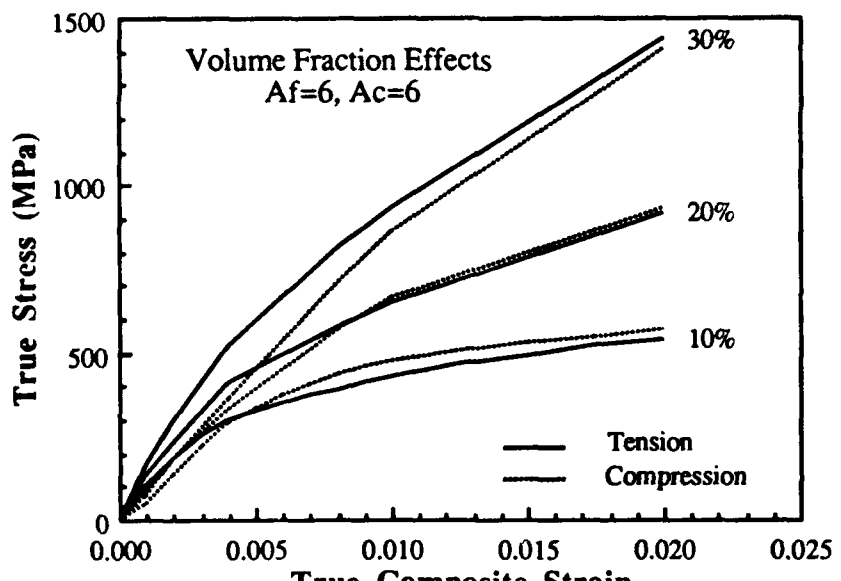
### 1. Fiber Volume Fraction Effects

#### a. Stress-Strain Behavior

To completely study the influence of thermal residual stresses on the stress-strain behavior of the MMC, the effect of increasing the fiber volume fraction in the composite was studied. Three aligned fiber models of the SiC whisker reinforced MMC (Figure 13a), with fiber aspect ratio and composite cell aspect ratio equal to six ( $A_f=A_c=6$ ), were constructed and numerically modelled in uni-axial compression and tension, with and without thermal residual stresses (TRS). MMC models with fiber volume fractions of 20 and 30 percent were compared to the 10 volume percent MMC previously discussed. It is seen from Figure 13b, that there is an overall increases in stiffness and strength with increasing fiber volume fraction and that residual stresses cause a significant difference in composite properties for the MMC in compression and tension. Most notably, the figure shows that for all MMC models, the elastic modulus in compression is substantially less than the modulus in tension when residual stresses are present.



(a)



(b)

**Figure 13.** Fiber Volume Fraction Effects: (a) Schematic of Model Configurations for Volume Fractions of 10%, 20% and 30% with  $A_f=A_c=6$  and (b) Composite Stress-Strain Behavior MMC With Residual Stresses in Tension and Compression.

Figure 14 shows a comparison of the stress-strain behavior of the 10, 20 and 30 vol.% MMC, with and without residual stresses. The 10 vol.% MMC (Figure 14a) exhibits greater strengthening in compression and less strengthening in tension with residual stresses present compared to the 10 vol.% MMC without residual stresses. The 20 vol.% MMC (Figure 14b) shows an intermediate behavior, where little strengthening is observed in compression or tension with residual stresses present, compared to the same MMC without residual stresses. The 30 vol.% MMC (Figure 14c), exhibits greater strengthening in tension and less strengthening in compression when residual stresses are present, which is contrary to the behavior of the 10 vol.% MMC.

To understand this significant fiber volume fraction effect, the 30 vol.% MMC has been studied and compared to the 10 vol.% MMC detailed in the previous section. The 30 vol.% MMC has a Young's modulus ( $E$ ), when residual stresses are present, of 144 GPa in tension, and 89 GPa in compression and when residual stresses are absent, a modulus of 131 GPa in both tension and compression. The 0.2 % offset yield stress (YS) is 780 MPa in tension, 1130 MPa in compression and 720 MPa without TRS. Figure 14c shows the MMC in compressive loading with TRS, with its significantly smaller modulus, increased yield strength and reduced flow stress.

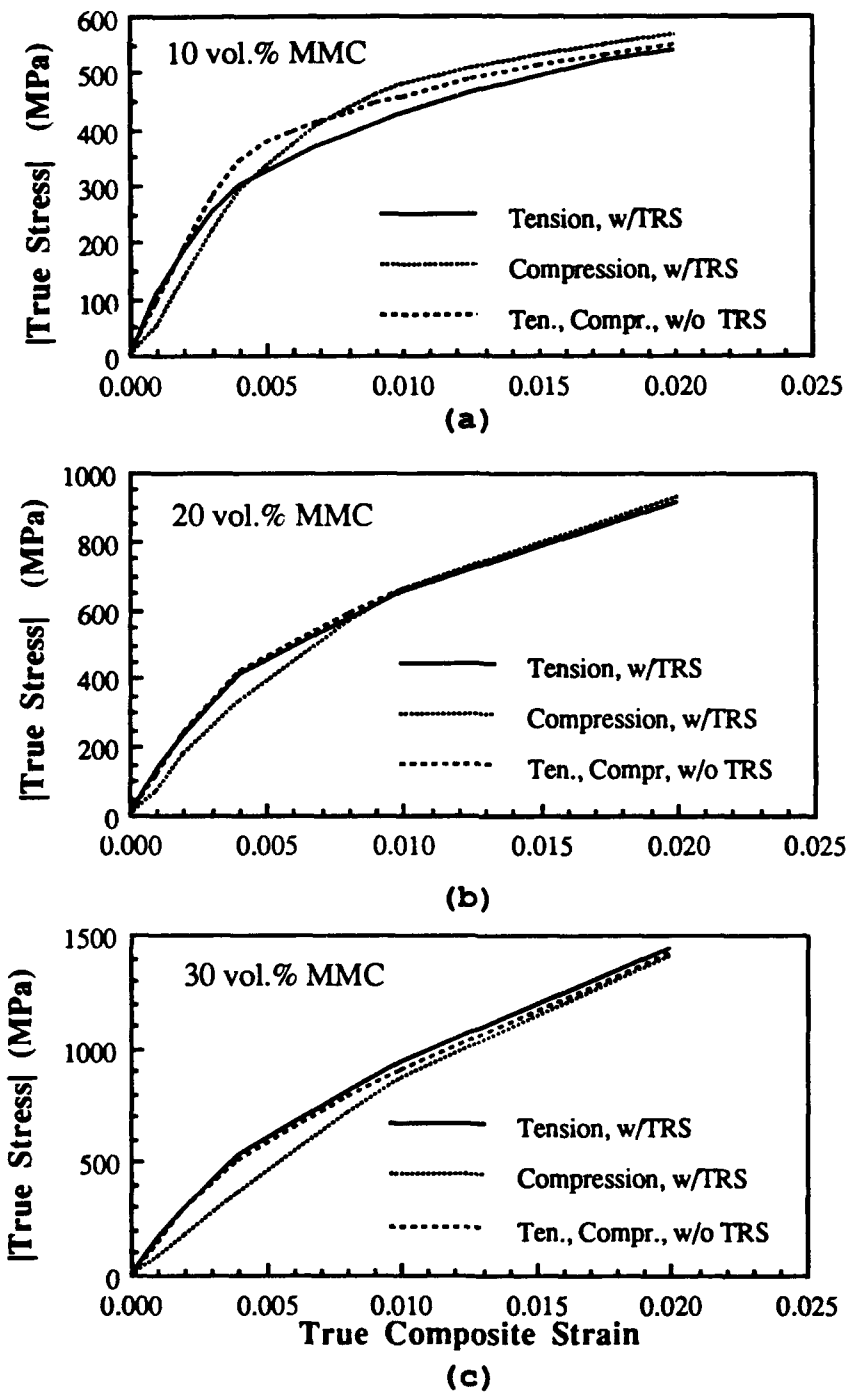
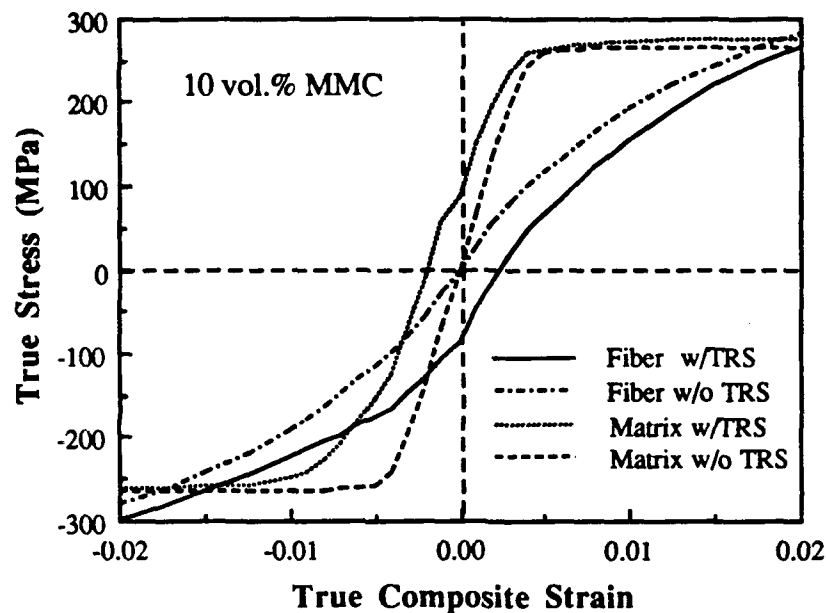
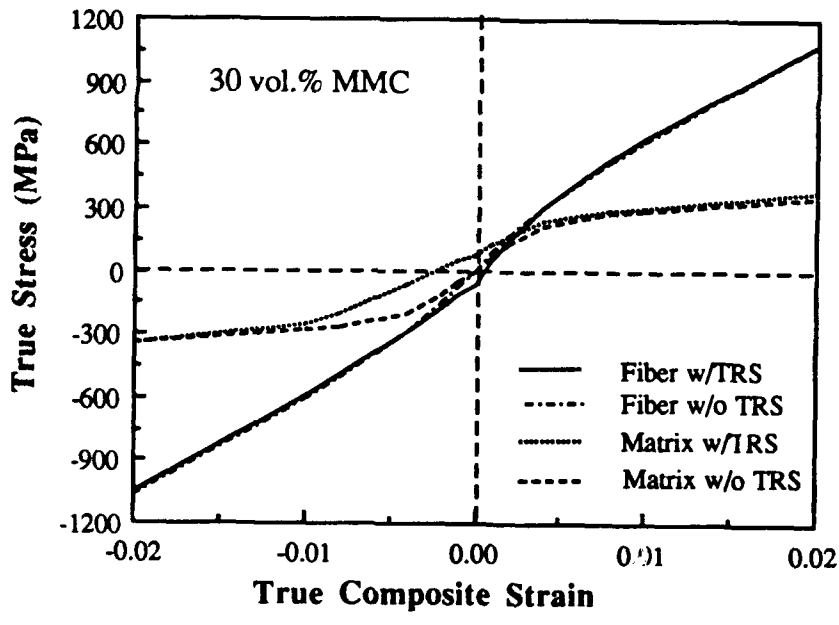


**Figure 14.** Fiber Volume Fraction Effects With and Without Residual Stresses: Composite Stress-Strain Curves in Tension and Compression for MMC with  $A_f = A_c = 6$  and Fiber Volume Fraction of (a) 10%, (b) 20% and (c) 30%

Figure 15 shows the stress-strain behavior of the fiber and matrix of the 10 vol.% MMC (Figure 15a) and the 30 vol.% MMC (Figure 15b). The 30 vol.% MMC fiber carries approximately the same stress both in the presence and absence of TRS, in tension and compression. This is very different from the behavior of the 10 vol.% MMC where the fiber in the as-quenched MMC carries more stress in compression and less stress in tension relative to the case without TRS. Accordingly, the behavior of the matrix is also different in the 30 vol.% MMC. The matrix in the as-quenched 30 vol.% MMC carries slightly more stress in tension relative to the case without TRS (similar to the 10 vol.% MMC). In compression, however, the matrix with TRS shows a substantially lower instantaneous modulus (or loading rate,  $d\sigma_c/d\epsilon_c$ ) than in the case without TRS, until  $\epsilon_c \approx -0.0125$ . This large difference in  $d\sigma_c/d\epsilon_c$  between the cases with and without TRS in the 30 vol.% MMC and the absence thereof in the 10 vol.% MMC is one reason for the observation that the composite flow stress in compression is less than that in tension in the 30 vol.% MMC (contrary to what is observed in the 10 vol.%). To better understand the origin of the low initial  $d\sigma_c/d\epsilon_c$  we will now investigate plastic deformation in the matrix of the 30 vol.% MMC.



(a)



(b)

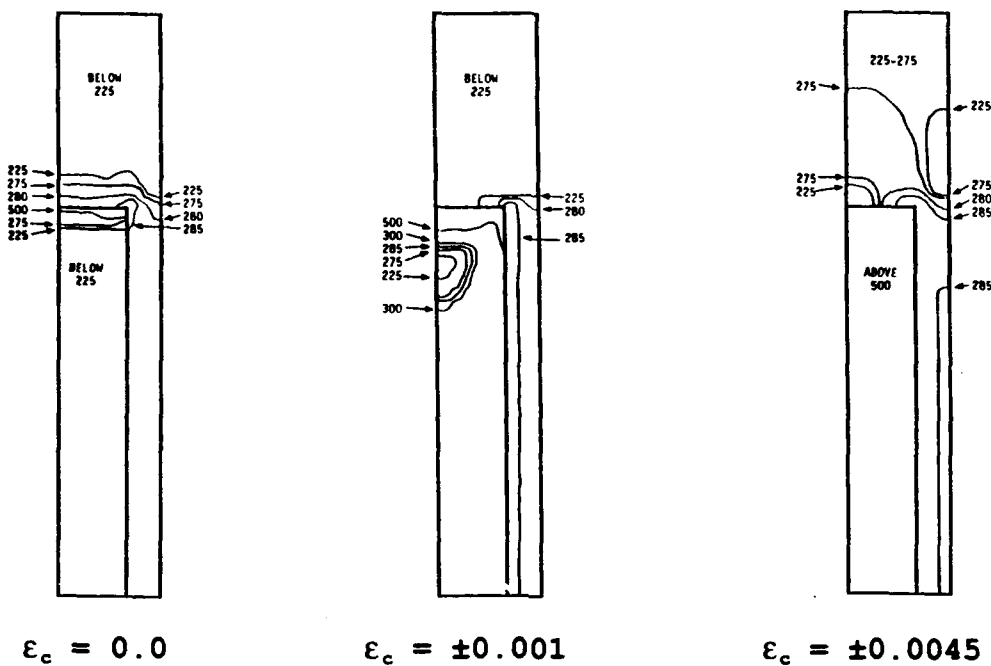
**Figure 15.** Fiber Volume Fraction Effects in Fiber and Matrix: Fiber and Matrix Stress-Strain Behavior With and Without Residual Stresses in Tension and Compression for Fiber Volume Fractions of (a) 10% and (b) 30%.

### **b. Plastic Zone Initiation and Growth**

Figure 16 shows a quarter cell of the 30 vol.% MMC with TRS at selected values of tension and compression. Iso-stress contours of Von Mises effective stress have been plotted for comparison with the 10 vol.% MMC effective stress contour plots (Figure 3 & 4). The 30 vol.% contour plot of the residual effective stress ( $\epsilon_c=0.0$ ) is similar to the 10 vol.% MMC with a plastically deformed matrix region surrounding the fiber, but with reduced effective stress in the fiber ( $\sigma_{eff}<225$  MPa).

The 30 vol.% MMC in tensile loading (Figure 16a) exhibits effective stress contour plots that closely resemble that of the 10 vol.% MMC. In compression, the effective stress contour plots (Figure 16b) reveal very different behavior than the 10 vol.% MMC. The entire matrix region above the fiber-tip plastically deforms at a strain of  $\epsilon_c=-0.001$ , in contrast to the tensile case, where the region does not completely deform until a strain beyond  $\epsilon_c=+0.0045$ . Additionally, in the 10 vol.% MMC this matrix region is not plastically deformed until  $\epsilon_c= 0.0045$  in tension and compression. This onset of large-scale plastic deformation in the matrix of the 30 vol.% MMC from the very early stages of compressive loading is the reason for the low initial loading rate ( $d\sigma_m/d\epsilon_c$ ) and the consequently lower flow stress in the presence of residual stresses.

**tension with residual stress**



**compression with residual stress**

**Figure 16.** Fiber Volume Fraction Effects - Plastic Zone Development: Von-Mises Effective Stress of 30 vol.% MMC With Residual Stresses in (a) Tension and (b) Compression.

### **c. Effective Plastic Strain**

Figure 17 shows the quarter cell models at a strain level of  $\epsilon_c = \pm 0.010$  in tension, compression and without residual stresses for the 10 vol.% MMC (Figure 17a) and the 30 vol.% MMC (Figure 17b) with iso-strain contours of cumulative effective plastic strain. The 30 vol.% MMC contour plots exhibit an higher overall cumulative effective plastic strain throughout the matrix, compared to the 10 vol.% MMC. This suggests that the overall work-hardenability ability of the matrix when loaded in both tension and compression increases with larger volume fraction, due to the smaller and therefore more constrained matrix of the MMC. Additionally, in compression, the 30 vol.% MMC exhibits a lower level of work-hardening in the matrix adjacent to the lateral fiber-matrix interface when compared to the MMC without TRS, which is not observed in the 10 vol.% MMC, and might indicate more effective matrix-to-fiber load transfer across the sidewall.

### **d. Fiber Loading**

Figure 18 shows the average axial fiber stress along half of the fiber length in the 10 vol.% MMC (Figure 18a) and the 30 vol.% MMC (Figure 18b) at selected increments of tension and compression. The residual axial fiber stresses ( $\sigma_{zzr}$ ) are significantly smaller in the 30 vol.% MMC than in the 10 vol.% MMC. Further, unlike the 10 vol.% MMC where the magnitude of the tensile fiber stress supported at a given

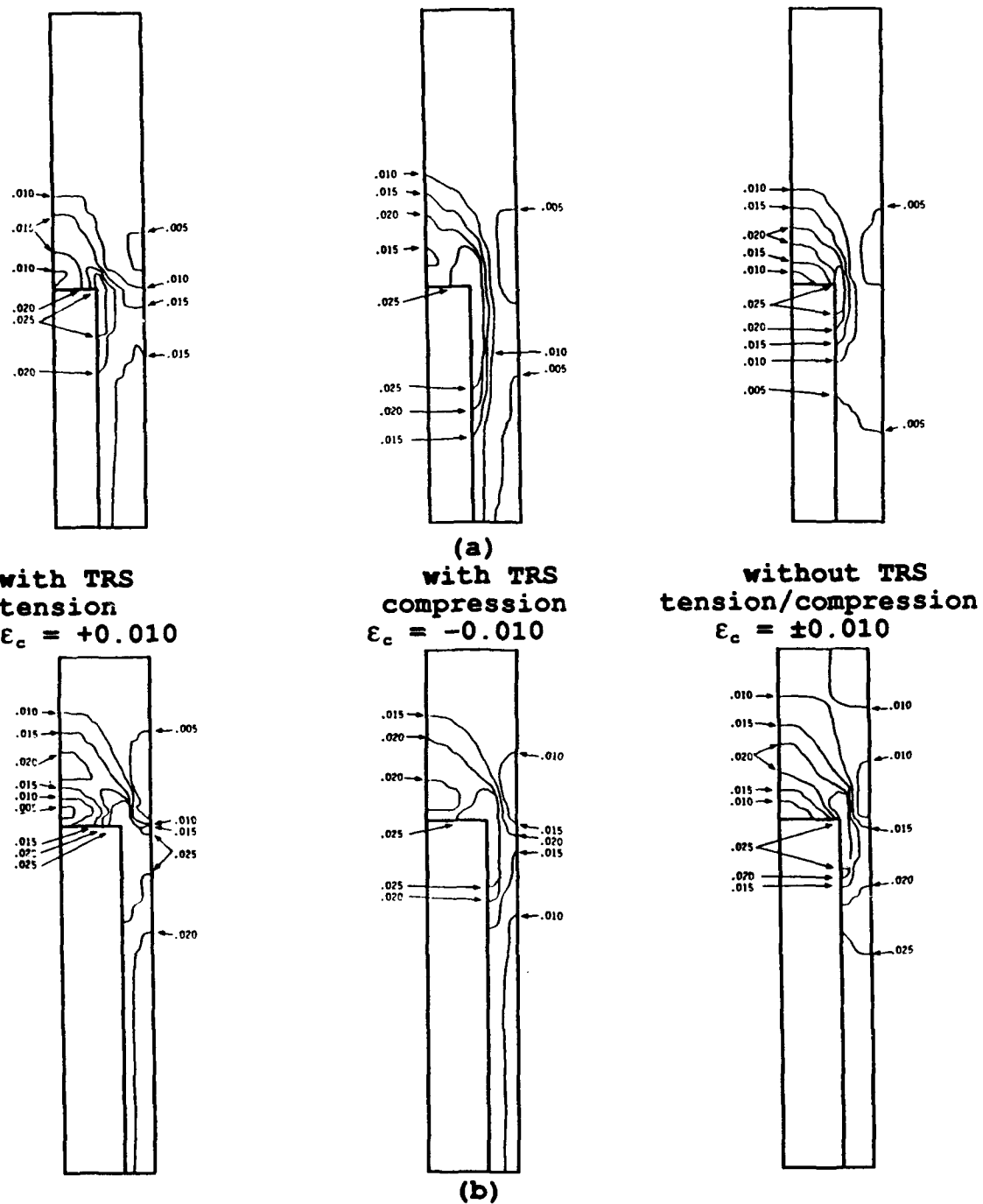
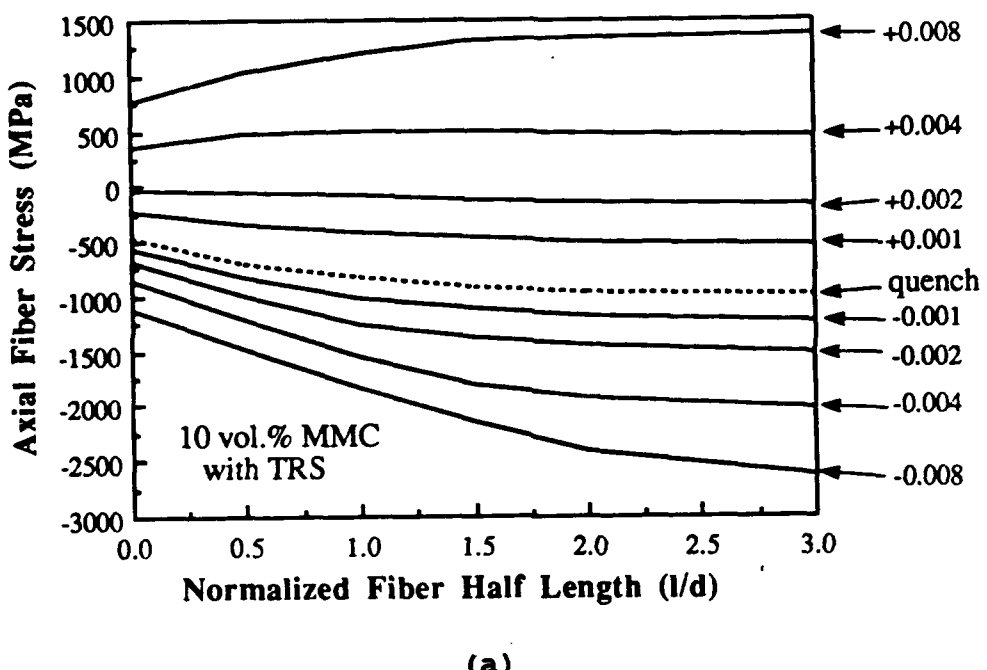
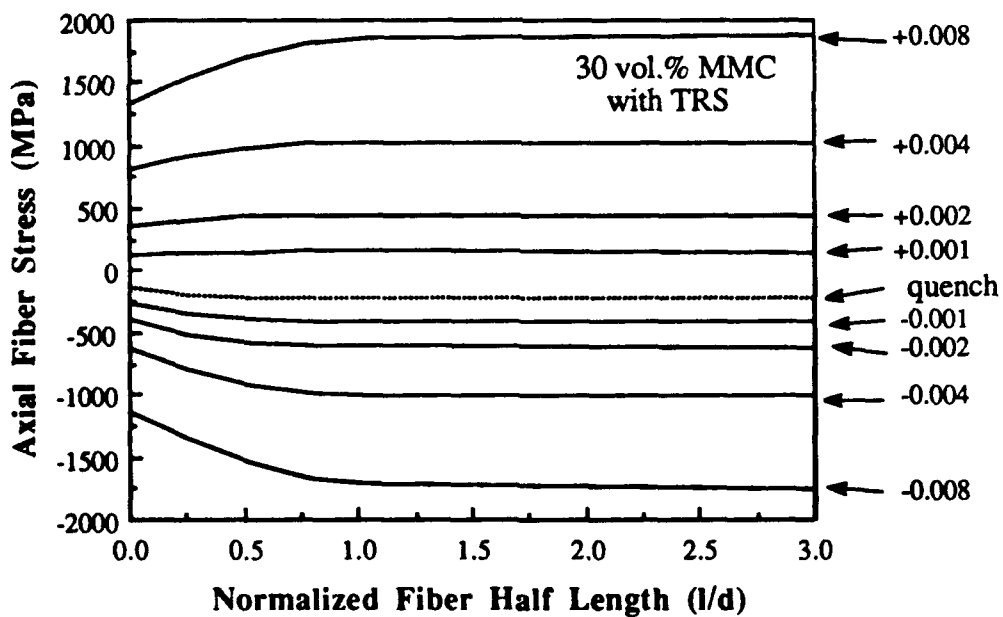


**Figure 17.** Cumulative Effective Plastic Strain: Effective Plastic Strain at Equivalent Values of Composite Strain ( $\epsilon_c=0.010$ ) in Tension with TRS, Compression With TRS, and Tension/Compression Without TRS for (a) 10 vol.% MMC and (b) 30 vol.% MMC with  $A_f=A_c=6$ .



(a)



(b)

**Figure 18.** Axial Fiber Stress With Residual Stresses: Axial Stress Carried by the Fiber at Indicated Composite Strains at Right in (a) 10 vol.% MMC and (b) 30 Vol.% MMC.

tensile strain is less than the magnitude of the compressive fiber stress supported at the same compressive strain, the magnitude of the tensile stress supported by the fiber of the 30 vol.% MMC at a given tensile strain is about equal to the magnitude of the compressive fiber stress supported at the same compressive strain. This indicates a smaller disparity in the load bearing ability of the fiber in tension and compression in the MMC with increasing fiber volume fraction.

In Figure 19, a comparison of axial fiber stress along half of the fiber length with and without TRS in tension (Figure 19a) and in compression (Figure 19b) shows that at a given strain the axial fiber stress supported by the fiber is nearly the same with and without TRS. This is not observed in the 10 vol.% MMC, which in tension and compression, exhibited a large stress between the presence and absence of residual stresses. It is suggested that TRS plays a less important role on fiber load-bearing ability with increasing fiber volume fraction in the MMC.

Figure 20 shows, specifically, the fiber-tip axial stress graphed for selected strain regimes in tension and compression, with and without TRS. The ordinate of the plots shows the increase in fiber-tip axial stress ( $\sigma_{zz}$ ) for given increases in the applied axial composite strain ( $\epsilon_c$ ). It is observed that the 10 vol.% MMC (Figure 20a) is nearly identical to the 30 vol.% MMC suggesting that although TRS significantly alter fiber-tip load transfer in compression and

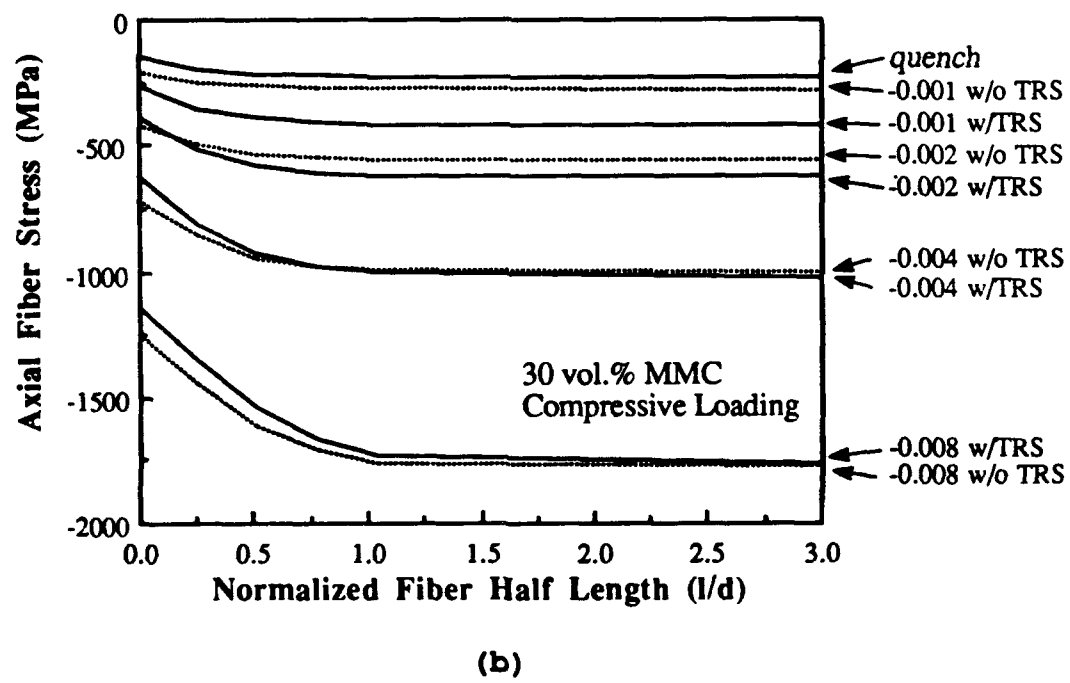
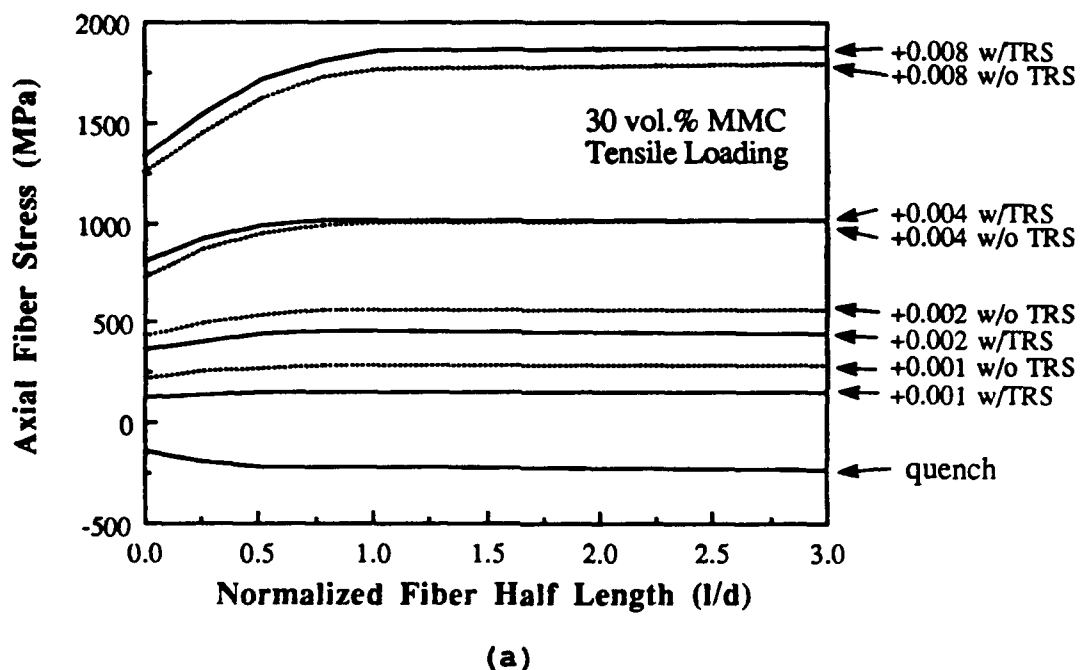
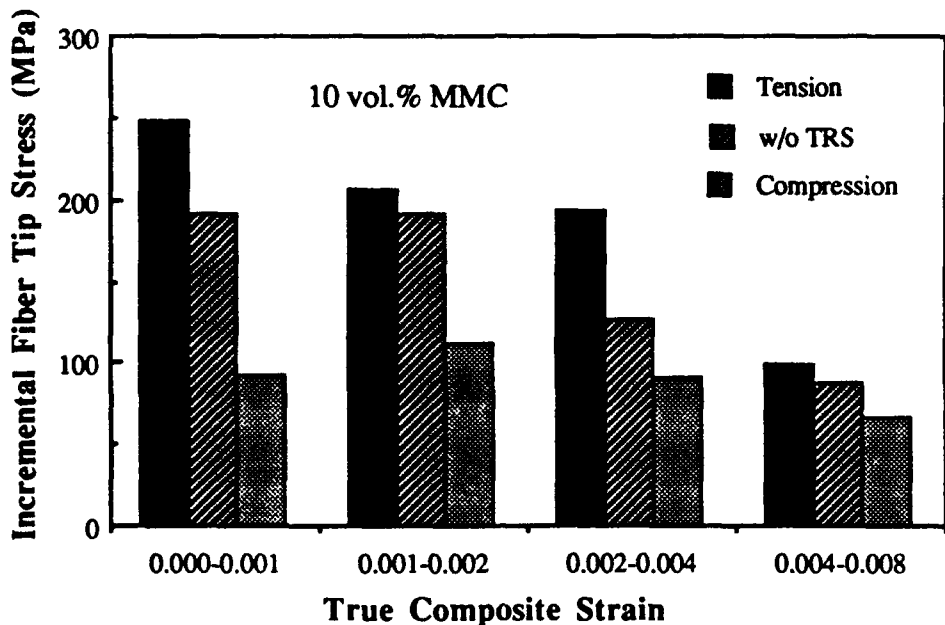
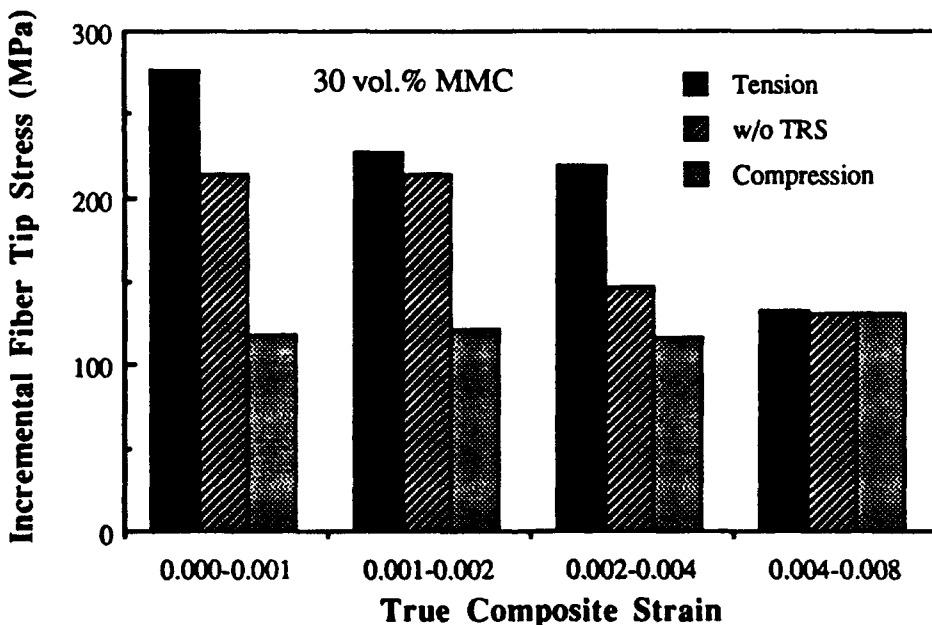


**Figure 19.** Axial Fiber Stress 30 vol.% MMC With and Without Residual Stresses: Axial Stress Carried by the Fiber in (a) Tension and (b) Compression.



(a)



(b)

**Figure 20.** Incremental Fiber Tip Stresses With and Without Residual Stress: Incremental Fiber-Tip Stress ( $\sigma_{zz(fiber-tip)} / \Delta \epsilon_c$ ) for Indicated Stress Regimes in (a) 10 vol.% MMC and (b) 30 vol.% MMC.

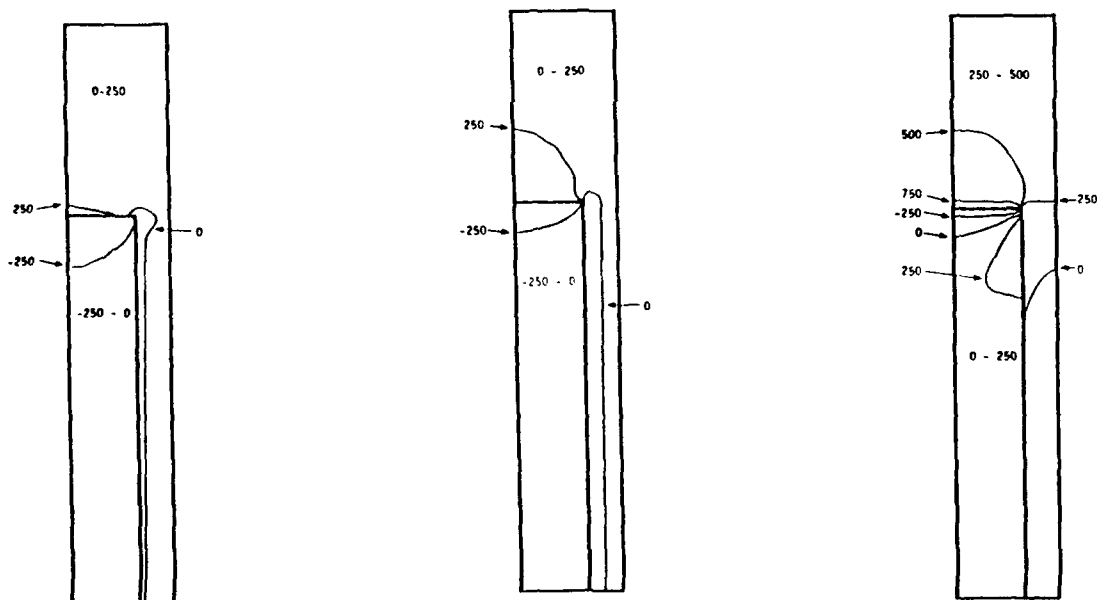
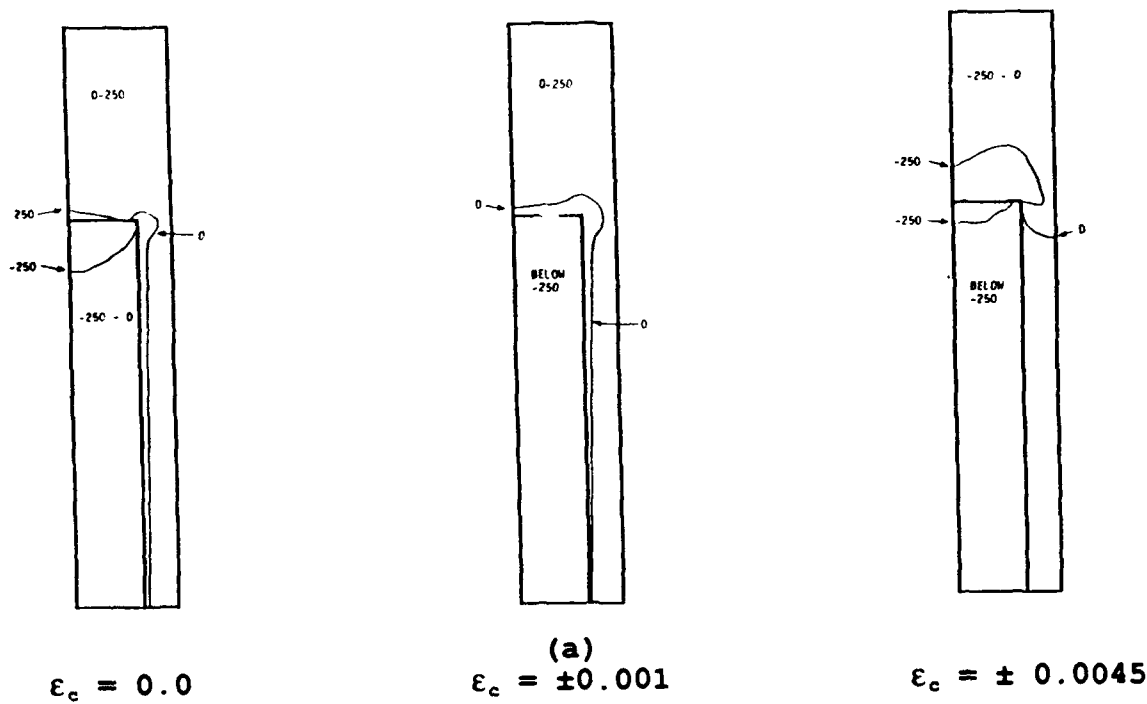
tension this phenomenon is not affected by fiber volume fraction.

#### e. **Hydrostatic Stress**

Figure 21 shows a quarter cell of the 30 vol.% MMC in tension (Figure 21a) and in compression (Figure 21b) TRS. The contour plots of hydrostatic residual stress ( $\epsilon_c=0.0$ ) shows that the matrix region above the fiber-tip is tensile with the highest stress at the fiber-matrix interface. This is not observed in the 10 vol.% MMC, which has a large compressive matrix above the fiber-tip. Under tensile strain ( $\epsilon_c=+0.001\&+0.0045$ ), both the tensile matrix region above the fiber-tip and the compressive matrix region adjacent to the lateral fiber-matrix interface expand, suggesting that crack nucleation in a MMC occurs first at the fiber-tip in tension as in the 10 vol.% MMC.

Under compressive strain ( $\epsilon_c=-0.001\&-0.0045$ ), the iso-stress contours of hydrostatic stress show that the tensile matrix region above the fiber-tip becomes compressive similar to the 10 vol.% MMC with a compressive matrix above the fiber-tip and tensile matrix region adjacent to the sidewall of the fiber, suggesting that interfacial decohesion is likely to occur at the lateral fiber-matrix interface in compressive loading. The crack nucleation behavior in the MMC does not exhibit any significant dependence on the fiber volume fraction.

tension, with residual stresses



compression, with residual stresses  
(b)

**Figure 21.** Hydrostatic Stress for a 30 vol.% MMC: Contours of Hydrostatic Stress With Residual Stresses for a 30 vol.% in (a) Tension and (b) Compression.

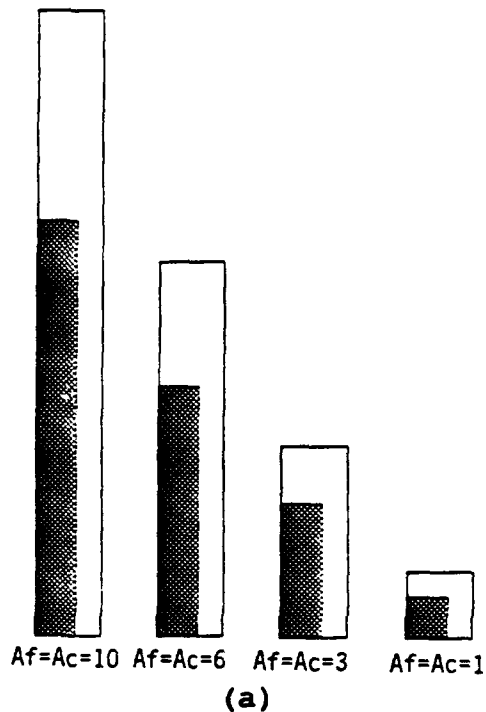
## **2. Fiber Aspect Ratio Effects**

### **a. Stress-Strain Behavior**

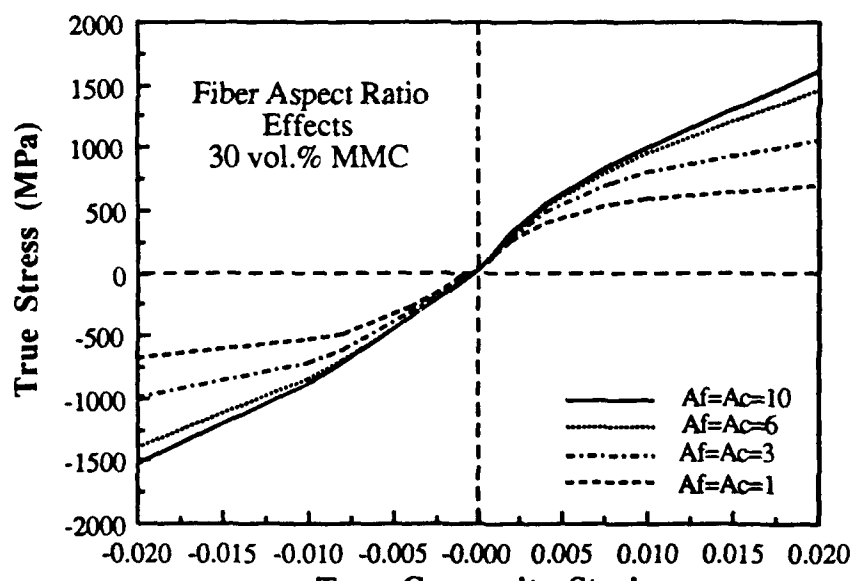
To understand the relationship between composite strength and fiber aspect ratio in the presence of residual stresses, four models of the 30 vol.% MMC were constructed and numerically modelled in tension and compression with residual stresses present (Figure 22a). The fiber aspect ratio and cell aspect ratio were set equal to one another to eliminate spacing effects ( $A_f=A_c$ ). Aspect ratio values of one, three, six, and 10 were modeled to simulate actual values. Figure 22b shows that the MMCs exhibited greater stiffness, yield strength, flow stress and work-hardening rates with increasing fiber aspect ratio in tension and compression. Additionally, it is observed that the strengthening is less pronounced as the fiber aspect ratio increases in tension and compression also. Comparing the compressive and tensile stress-strain behavior of equivalent MMC reveals strength differential effects, specifically in elastic modulus, similar to the effect discussed in the previous section.

### **b. Fiber Loading Rate Behavior**

Figure 23 shows the fiber stress-strain behavior for 10 vol.% and 30 vol.% MMC with two equivalent fiber-cell aspect ratios ( $A_f=A_c$ ) of three and six. It is observed that the stress carried by the fiber increases with increasing fiber aspect ratio and larger fiber volume fraction. In tension, the



(a)



(b)

**Figure 22. Fiber Aspect Ratio Effects:** (a) Schematic of Model Configuration for 30 vol.% MMC with  $A_f = A_c = 10$ , 6, 3, and 1, and (b) Composite Stress-Strain Behavior in Tension and Compression in the Presence of Residual Stresses.

fiber loading is initially dependent on fiber volume fraction and only at strains  $\epsilon_c > +0.004$  does the fiber aspect ratio play an important role in the fiber loading behavior. In compression, the fiber loading is initially dependent on both fiber volume fraction and fiber aspect ratio, even though the compressive stress-strain behavior of the fibers at larger strains  $\epsilon_c > -0.010$  are similar to the tensile behavior.

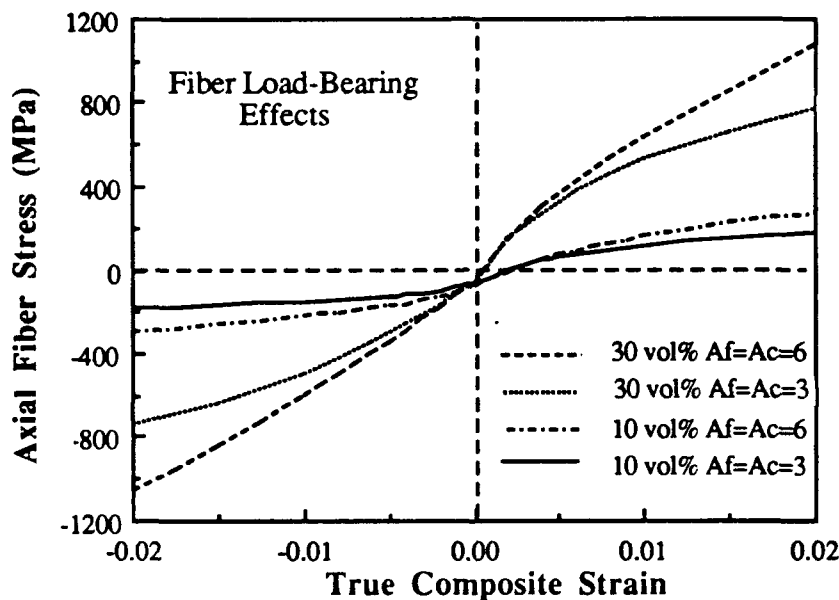


**Figure 23. Fiber Load-Bearing Behavior: Effect of Fiber Aspect Ratio and Volume Fraction on the Stress Carried by the Fiber with Residual Stresses.**

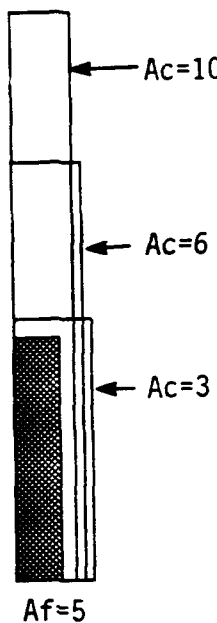
### 3. Cell Aspect Ratio Effects

The effect of fiber spacing was studied using three 30 vol.% MMC models (Figure 24a) with a fiber aspect ratio of five ( $A_f=5$ ) and a composite cell aspect ratios ( $A_c$ ) of three,

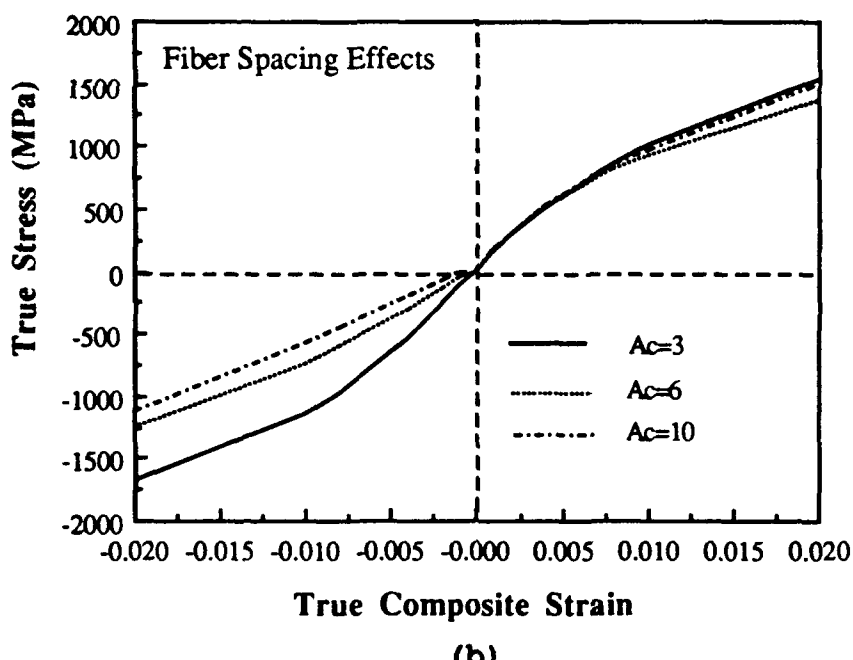
six, and 10. Figure 24b shows the composite stress-strain behavior in tension and compression with residual stresses present. In tension, fiber spacing has no appreciable effect on composite stiffness. However, in MMCs with close end-to-end and side-to-side spacing an increase in composite work-hardening is observed due to additional matrix constraint, which results in somewhat larger plastic strains, and consequently slightly higher matrix flow stress. In compression, fiber spacing has a large effect on both the stiffness and flow stress of the MMC. It is suggested that in compression there is enhanced load transfer through the sidewall, therefore the matrix next to the lateral fiber-matrix interface, which is volumetrically larger for  $A_c=3$  bears little load, with the fiber bearing a correspondingly large load. Hence  $A_c=3$  shows the largest strength in compression. Likewise,  $A_c=10$  which has the least matrix volume next to the lateral interface, should have the lowest strength in compression.

### C. EXPERIMENTAL RESULTS

In order to numerically model a composite material accurately, the model must be similar both geometrically and materially to the actual composite. Figure 25 shows a SEM micrograph of a 30 vol.  $\text{SiC}_w/\text{Al}$  6061 composite. The picture exhibits three important aspects of the actuals composite; First, there is a significant degree of randomness in fiber



(a)



(b)

**Figure 24.** Fiber Spacing Effects: (a) Schematic of Fiber Spacing Models With  $Af=5$  and  $Ac=3$ , 5, and 10 and (b) Composite Stress-strain Behavior in Tension and Compression with Residual Stresses.

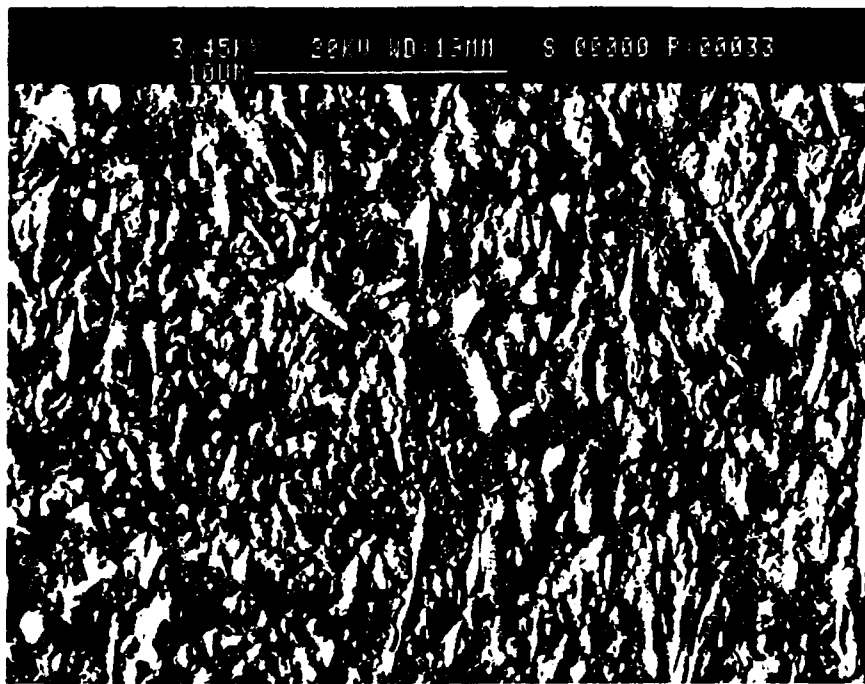


**Figure 25.** SEM Micrograph: Scanning Electron Microscopy Photography at 3,45 KX of a 30 vol.% SiC Fiber-Reinforced Al 6061 Composite With a 6.5:1 Reduction Ratio.

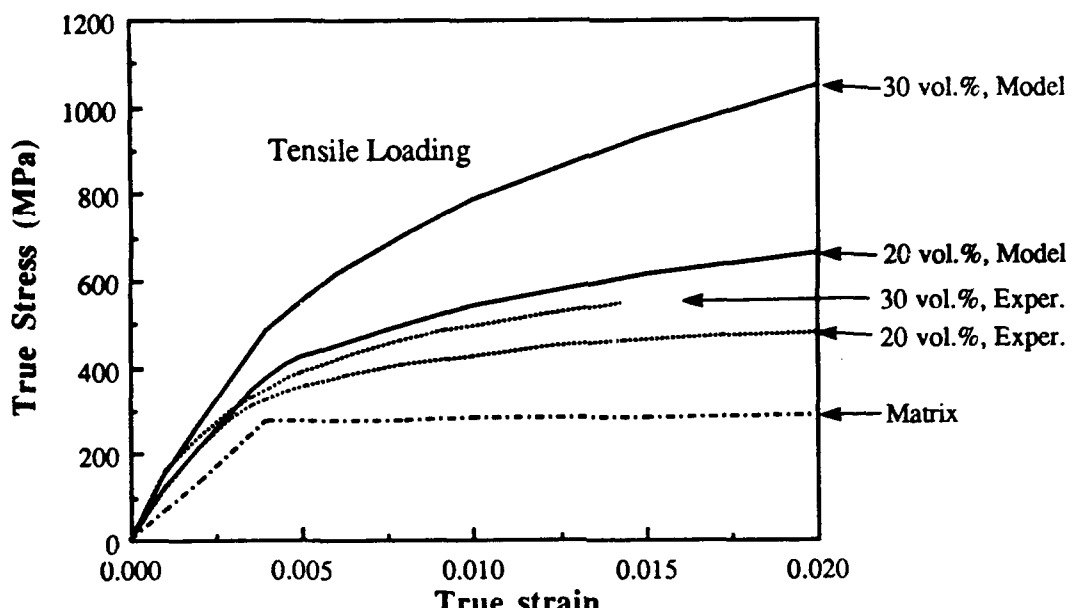
alignment. Second, there is a non-uniformity (clustering) in fiber distribution throughout the material, and third, there is a wide range of fiber aspect ratios encountered in the material. Takao et al. [Ref. 29] found that fiber alignment had a greater effect on composite elastic modulus than volume fraction. Christman et al. [Ref. 19] found that clustering greatly reduced the resistance to plastic flow in the composite by decreasing the magnitude of matrix triaxiality. Takao and Taya [Ref. 30] found that the wider the

range of aspect ratio, the greater the error in the use of average aspect ratio in analytical results.

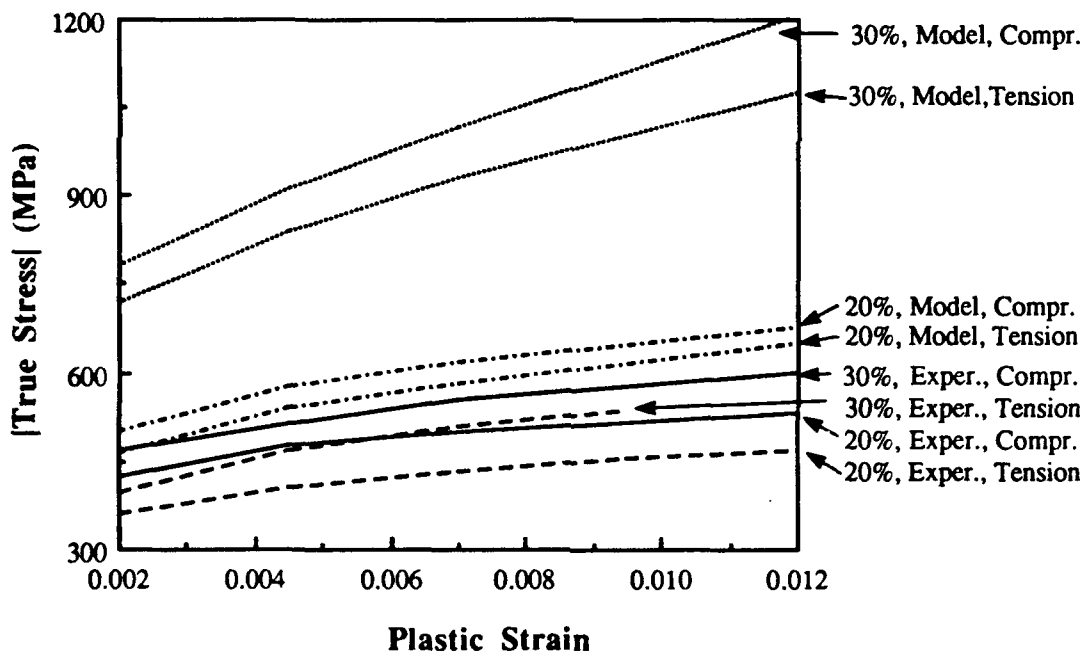
From Figure 25 the average composite fiber aspect ratio was estimated to be about 2.2 with a low of 1.0 and a high of 22.9. This estimate is expected to be low due to fiber misalignment. The numerical model with fiber aspect ratio and cell aspect ratio set at three was determined to best represent the actual composite.

Figure 26a shows the analytical results in tension and the tensile experimental results for both the 20 and 30 vol.% MMC, it was found that the aligned fiber model overpredicts both the yield strength and work-hardening rate of the actual composite. This can be attributed to the fact that the model assumes perfectly aligned, parallel fibers, which is clearly not the actual case (Figure 25). Additionally, the model ignores effects of clustering, which is known to reduce the resistance to plastic flow [Ref. 19], and the interfacial decohesion, which is probably of importance in actual composites.

The tensile and compressive results for both the numerical models and the experimental testing are shown in Figure 26b, where composite flow stress versus plastic strain is plotted. The numerical model predicts the higher yield strength in compression than in tension and a higher yield strength and work-hardening rate with increasing fiber volume fraction, similar to the actual composite behavior. The 20 vol.% model



(a)



(b)

**Figure 26.** Experimental Testing Results: Comparison of Experimental Testing and Numerical Results in (a) Tensile Loading and (b) Tensile and Compressive Loading With Plastic Strain on the Horizontal Axis.

exhibits better experimental correlation than the 30 vol.% MMC, which can be expected due to the mismatch between fiber aspect ratio and fiber spacing assumed in the model and that occurring in the actual composite. The greater level of error in models with higher volume fractions can probably be attributed to the reduced lateral and longitudinal spacing between the fiber and the cell, which results in increased levels of matrix constraint, and hence has a significant effect on the plastic flow behavior of the material.

#### **IV. CONCLUSIONS**

The uniaxial stress-strain response of a SiC<sub>w</sub>/Al 6061 composite was investigated to assess the role of thermal residual stresses on the constitutive behavior of the material. The following summarizes the relevant findings of the phenomenological study and the parametric study:

##### **A. EFFECT OF THERMAL RESIDUAL STRESSES**

1. Elastic-plastic and thermo-elastic-plastic analysis using finite-element models of fiber reinforced metal-matrix composites can be used to predict trends in the uniaxial stress-strain behavior given the thermo-mechanical properties of the constituent phases as a starting point. However, exact correlation with actual experimental results is difficult since several idealistic assumptions which are made for modeling expediency are often not satisfied in real composites. This usually translates into overestimation of the composite strength and stiffness properties resulting from the model.
2. Residual stresses significantly impact the stress-strain behavior of the composite, principally by affecting the load transfer characteristics between the matrix and the fiber.
3. Residual stresses affect the initiation and continuation of plastic deformation in the matrix by producing an initial plastic zone adjacent to the fiber/matrix interface that is affected somewhat differently in compression than it is in tension.
4. Residual stresses affect the fiber load transfer characteristics at the fiber tip, increasing load transfer through the fiber ends in tension and decreasing it in compression.

5. Residual stresses resulting in a negative hydrostatic stress state in certain locales of the matrix adjacent to the fiber-matrix interface may impede decohesion at the interface.

## **B. PARAMETRIC STUDY**

1. The stiffness, yield strength and work-hardening rate of the composite increase with increasing fiber volume fraction and fiber aspect ratio in tension and compression.
2. The strength differential effect produced by residual stresses is less pronounced with increasing fiber volume fraction.
3. Variations in lateral fiber spacing have little effect in tension, but have significant effect in compression on composite properties.

## APPENDIX A: SAMPLE ADINA INPUT FILE

```
* THIS INPUT FILE SIMULATES THERMAL AND TENSILE LOADING OF A
* METAL-MATRIX COMPOSITE. THE PROGRAM INCLUDES COMMENTS AT
* APPROPRIATE LOCATIONS TO ILLUSTRATE SOME OF THE IMPORTANT
* FEATURES OF ADINA IN NON-LINEAR ANALYSIS.
*
* THE FOLLOWING BLOCK OF CODE CONTAINS ADINA CONTROL INFORMATION
DATABASE CREATE
CONTROL ORIGIN=UPPERLEFT PLOTUNIT=CM
FILEUNITS LIST=6 LOG=6 ECHO=6
*
* THE FOLLOWING BLOCK OF CODE CONTAINS SPECIFICATIONS FOR MODEL DEGREES OF
* FREEDOM, SOLUTION TIME PERIOD LENGTH AND TIME-STEP SIZE. THE FIRST
* "MASTER" COMMAND LINE IS USED IN ELASTOPLASTIC ANALYSIS; THE SECOND
* COMMAND SIMULATES THE QUENCH PROCESS AND THE THIRD SIMULATES THE
* TENSILE LOADING FOLLOWING THE QUENCH.
* CAN BE USED IN DURING A GIVEN RUN, THE OTHER MUST BE COMMENTED OUT USING
* A '*'.
MASTER IDOF=100111 ITP56=0 NSTEP=6 DT=1.0
*MASTER IDOF=100111 ITP56=2 NSTEP=1 DT=1.0
*MASTER IDOF=100111 ITP56=2 NSTEP=6 DT=1.0
*
* THE FOLLOWING BLOCK OF CODE CONTAINS THE KINEMATIC AND ITERATION METHOD
* SPECIFICATIONS. AUTOMATIC-ATS IS A FEATURE USED IN NON-LINEAR ANALYSIS
* TO ASSIST IN ACHIEVING THE REQUIRED TOLERANCE FOR THE OUT-OF-BALANCE
* ENERGY NORM.
KINEMATICS DISP=LARGE STRAINS=LARGE
ITERATION METHOD=FULL-NEWTON LINE-SEARCH=YES
AUTOMATIC-ATS N=10
*
* THE FOLLOWING COMMANDS RELATE TO THE PROGRAM OUTPUT. COMMENT IN THE
* "WORKSTATION" COMMAND IF A HARDCOPY OF THE MODEL CONFIGURATION IS
* DESIRED.
HEADING 'VF=30% AF=3 AC=3'
PRINTOUT VOLUME=MAX
PORTHOLE FORMATTED=YES FILE=60
*WORKSTATION SYSTEM=4 DEVICE=0 OPTION=0
*
* THE FOLLOWING CODE SPECIFIES THE NATURE OF THE APPLIED TEMPERATURE LOAD.
* NUMBERS TO THE LEFT ARE TIME VALUES AND THE NUMBERS TO THE RIGHT ARE THE
* VALUES OF TEMPERATURE CHANGE FROM THE INITIAL TEMPERATURE OF THE MODEL.
TIMEFUNCTION 1
 0.0      0.0
 1.0     -505.0
*
* THE FOLLOWING TIME FUNCTIONS REPRESENT THE DISPLACEMENT LOADING SEQUENCE
* THE NUMBERS TO THE RIGHT ARE DISPLACEMENTS FROM THE REFERENCE LENGTH OF
* THE MODEL THAT CORRESPOND TO A GIVEN LOGARITHMIC STRAIN TO BE USED IN
* THE STRESS-STRAIN CURVE. NOTE: THE DISPLACEMENTS FOR THE MODEL WITH
* RESIDUAL STRESSES START AT TIME=2.0 SINCE THE QUENCH PROCESS OCCURRED
* FROM TIME 0 to 1.0. IN ADDITION, THE DISPLACEMENTS ARE INITIALLY
* NEGATIVE DUE TO THE QUENCH PROCESS. THE SUBSEQUENT DISPLACEMENTS
```

\* ARE ADDED TO THE NEW REFERENCE. THE DISPLACEMENT SPECIFICATIONS  
\* IN ADINA ARE ALWAYS ABSOLUTE DISPLACEMENTS, MEANING THAT A RELATIVE  
\* CHANGE IN DISPLACEMENT CANNOT BE INPUT.

\*

\*\*\* ALIGNED TENSION WITH RESIDUAL STRESS \*\*\*

TIMEFUNCTION 2

0.0	0.0
2.0	-.0244957
3.0	-.0200380
4.0	-.0111091
5.0	-.00216242
6.0	0.00680222
7.0	0.0157848

\*

\*\*\* ALIGNED COMPRESSION WITH RESIDUAL STRESS \*\*\*

TIMEFUNCTION 3

0.0	0.0
2.0	-.0333978
3.0	-.0378422
4.0	-.0467167
5.0	-.0555754
6.0	-.0644154
7.0	-.0732238

\*

\*\*\* ALIGNED WITHOUT RESIDUAL STRESS \*\*\*

TIMEFUNCTION 4

0.0	0.0
1.0	0.00448224
2.0	0.00896897
3.0	0.0179559
4.0	0.0269608
5.0	0.0359837
6.0	0.0450247
7.0	0.0677065

\*

\* THE FOLLOWING BLOCK OF CODE INPUTS THE NODAL COORDINATES AND SPECIFIES  
\* THE NUMBER OF ELEMENTS DESIRED BETWEEN NODES.

SYSTEM 1 TYPE=CARTESIAN

COORDINATES

ENTRIES	NODE	Y	Z
	1	1.49	4.48
	2	1.0	4.48
	3	0.0	4.48
	4	1.49	3.0
	5	1.0	3.0
	6	0.0	3.0
	7	1.49	2.24
	8	1.0	2.24
	9	0.0	2.24
	10	1.49	0.0
	11	1.0	0.0
	12	0.0	0.0

```

*
LINE STRAIGHT 1 2 EL=3
LINE STRAIGHT 2 3 EL=6
LINE STRAIGHT 4 5 EL=3
LINE STRAIGHT 5 6 EL=6
LINE STRAIGHT 7 8 EL=3
LINE STRAIGHT 8 9 EL=6
LINE STRAIGHT 10 11 EL=3
LINE STRAIGHT 11 12 EL=6
*
LINE STRAIGHT 1 4 EL=9
LINE STRAIGHT 4 7 EL=5
LINE STRAIGHT 7 10 EL=14
LINE STRAIGHT 2 5 EL=9
LINE STRAIGHT 5 8 EL=5
LINE STRAIGHT 8 11 EL=14
LINE STRAIGHT 3 6 EL=9
LINE STRAIGHT 6 9 EL=5
LINE STRAIGHT 9 12 EL=14
*
* THE FOLLOWING CODE DEFINES MATERIAL PROPERTIES TO BE USED IN THE MODEL.
* THE FIRST MATERIAL SPECS CORRESPOND TO THE FIBER AND THE SECOND TO THE
* ALUMINUM MATRIX. EACH SET CONTAINS THE CORRESPONDING COMMANDS FOR
* ELASTOPLASTIC ANALYSIS. THE "TREF" COMMAND MUST BE SET TO 530.0 FOR THE
* QUENCH RUN AND 25.0 FOR THE SUBSEQUENT TENSILE DISPLACEMENT RUN.
MATERIAL 1 THERMO-ELASTIC TREF=530.0
    0.0 450E9 0.2 4.3E-6
    1000.0 450E9 0.2 4.3E-6
*MATERIAL 1 ELASTIC E=450E9 NU=0.2
*
MATERIAL 2 THERMO-PLASTIC TREF=530.0
    0.0 68.3E9 0.33 276E6 656E6 23.0E-6
    1000.0 68.3E9 0.33 276E6 656E6 23.0E-6
*MATERIAL 2 PLASTIC E=68.3E9 NU=0.33 Y=276E6 ET=656E6
*
* THE FOLLOWING CODE SELECTS GRCPUS OF ELEMENTS IN THE MODEL AND ASSIGNS
* THEM PREVIOUSLY DEFINED MATERIAL PROPERTIES
EGROUP 1 TWODSOLID SUB=0 M=1
GSURF 5 6 9 8   EL1=6 EL2=5 NODES=4
GSURF 8 9 12 11 EL1=6 EL2=14 NODES=4
*
EGROUP 2 TWODSOLID SUB=0 M=2
GSURF 1 2 5 4   EL1=3 EL2=9 NODES=4
GSURF 2 3 6 5   EL1=6 EL2=9 NODES=4
GSURF 4 5 8 7   EL1=3 EL2=5 NODES=4
GSURF 7 8 11 10 EL1=3 EL2=14 NODES=4
*
* THE FOLLOWING CODE CONTAINS THE BOUNDARY CONDITION SPECIFICATIONS. THE
* FOLLOWING CONDITIONS ARE APPLICABLE FOR THE ALIGNED FIBER MODEL.
* APPENDIX B CONTAINS A SECTION OF CODE ILLUSTRATING THE
* APPROPRIATE MODIFICATIONS FOR THE STAGGERED FIBER MODEL.

```

```
BO 111111 NODES
 12
BO 101111 NODES
 10 / 11
 34 TO 40
BO 110111 NODES
 3 / 6 / 9
 89 TO 112
*
CONSTRAINT
 1 3 3 3 3 TO 2 3 3 3 3
 13 3 3 3 3 TO 19 3 3 3 3
 1 2 10 2
 4 2 10 2
 7 2 10 2
 41 2 10 2 TO 64 2 10 2
*
* THE FOLLOWING COMMANDS DEFINE THE TYPE OF LOADING TO BE APPLIED TO THE
* MODEL. THESE COMMANDS ARE USED IN CONJUNCTION WITH THE TIMEFUNCTION
* COMMANDS DISCUSSED PREVIOUSLY. IT IS IMPORTANT TO NOTE THAT IF THE
* APPLIED LOADING IS STATIC (I.E. TIME INDEPENDENT) THEN THE TIME VALUES
* IN THE TIME FUNCTION COMMAND REPRESENT LOAD STEPS.
LOADS TEMPERATURE TREF=530
 1 1.0 1 TO 280 1.0 1
*
LOADS DISPLACEMENT
 3 3 1.0 2
*
* THE FOLLOWING COMMANDS ALLOW THE INPUT NODE AND ELEMENT CONFIGURATION
* FOR THE MODEL TO BE DISPLAYED ON THE SCREEN AS LONG AS THE "WORKSTATION"
* COMMAND IS COMMENTED OUT.
FRAME HEADING=UPPER XSF=1.0 YSF=0.5 XFMAX=22.5 YFMAX=17.0
MESH NODES=11 ELEMENT=1
*
ADINA
END
```

## APPENDIX B: DATA REDUCTION PROGRAMS

The following programs were used to reduce the ADINA output file to data points to be plotted on stress-versus-strain curves.

```
C THIS PROGRAM READS THE ADINA OUTPUT FILE AND COMBINES THE STRESS VALUES
C WITH THE ELEMENTAL VOLUMES TO PRODUCE A VOLUME-AVERAGED VALUE OF AXIAL
C STRESS.
C
C      PROGRAM TEST
C      CALL INIT
C      CALL READ
C      STOP
C      END
C
C      THIS SUBROUTINE ZEROS OUT ARRAYS AND READS THE VOLUME DATA FILE.
C      THE PARAMETER VARIABLES ARE: NUMBER OF ELEMENTS (NEL), NUMBER OF LOAD
C      STEPS (LC) AND NUMBER OF ELEMENTS IN THE FIBER (NFBR).
C
C      SUBROUTINE INIT
C      PARAMETER (NEL=252,LC=6,NFBR=114)
C      REAL SZ(1:NEL,1:4),SZBAR(1:LC),V(1:NEL),FBR(1:NFBR)
C      COMMON // SZ,SZBAR,V,FBR
C
C      DO 10 I=1,NEL
C      V(I)=0.0
C      DO 15 J=1,4
C      SZ(I,J)=0.0
C 15    CONTINUE
C 10    CONTINUE
C
C      DO 20 K=1,LC
C      SZBAR(K)=0.0
C      FBR(K)=0.0
C 20    CONTINUE
C
C      OPEN (01,STATUS='OLD')
C      DO 25 L=1,NEL
C      READ (01,*,END=50) V(L)
C 25    CONTINUE
C
C      PRINT *, 'EOF VOL.DAT'
C
C      RETURN
C      END
C
C      THIS SUBROUTINE READS THE FORMATTED ADINA OUTPUT FILE, AFTER THE HEADERS
C      HAVE BEEN REMOVED, AND CALCULATES THE AVERAGE Z STRESS IN EACH ELEMENT
C      BY AVERAGING THE FOUR STRESS VALUES AT THE GAUSS POINTS.  THIS AVERAGE
```

C STRESS IS MULTIPLIED BY ITS ELEMENTAL VOLUME AND SUMMED OVER THE ENTIRE  
C VOLUME OF THE MODEL. THE OUTPUT IS TWO FILES: ONE CONTAINING THE  
C COMPOSITE STRESS VALUES AT THE GIVEN LOAD LEVELS AND ONE CONTAINING  
C THE STRESS LEVELS IN THE FIBER AT THE SAME LOAD LEVELS.

C

```
SUBROUTINE READ
PARAMETER (NEL=252,LC=6,VOL=4.97,NFBR=114)
REAL SZ(1:NEL,1:4),SZBAR(1:LC),V(1:NEL),FBR(1:NFBR)
CHARACTER*8 STATE
COMMON // SZ,SZBAR,V,FBR

C
OPEN (02,STATUS='OLD')
OPEN (03,FILE='V30.DAT',STATUS='NEW')
OPEN (04,FILE='V30_FBR.DAT',STATUS='NEW')

C
DO 20 K=1,LC
SUM=0.0
DO 25 L=1,NEL
READ (02,*) IEL
READ (02,21) INR,INS,STATE,SX,SY,SZ(L,1),SYZ,SVM,SMAX
READ (02,*) SYS,SMIN
READ (02,*)
READ (02,21) INR,INS,STATE,SX,SY,SZ(L,2),SYZ,SVM,SMAX
READ (02,*) SYS,SMIN
READ (02,*)
READ (02,21) INR,INS,STATE,SX,SY,SZ(L,3),SYZ,SVM,SMAX
READ (02,*) SYS,SMIN
READ (02,*)
READ (02,21) INR,INS,STATE,SX,SY,SZ(L,4),SYZ,SVM,SMAX
READ (02,*) SYS,SMIN
READ (02,*,END=50)
READ (02,*,END=50)
21 FORMAT (14X,I1,3X,I1,5X,A8,5X,4(E12.5,2X),5X,2(E12.5,4X))
C
SBAR=((SZ(L,1)+SZ(L,2)+SZ(L,3)+SZ(L,4))/4.0)*V(L)
C
SUM=SUM+SBAR
C
IF (L.EQ.NFBR) THEN
FBR(K)=SUM/VOL
ENDIF
25 CONTINUE
SZBAR(K)=SUM/VOL
20 CONTINUE
C
50 PRINT *, 'EOF DETECTED'
C
DO 35 N=1,LC
WRITE (03,*) SZBAR(N)
WRITE (04,*) FBR(N)
35 CONTINUE
RETURN
END
```

```

C THIS PROGRAM CALCULATES ELEMENTAL VOLUMES BASED ON THE GEOMETRY OF THE
C FINITE-ELEMENT MODEL. THE REQUIRED INPUTS ARE:
C           NX: NUMBER OF ELEMENTS IN THE MODEL IN THE HORIZ. DIRECTION.
C           NY: NUMBER OF ELEMENTS IN THE MODEL IN THE VERT. DIRECTION.
C           NFX: NUMBER OF FIBER ELEMENTS IN THE HORIZ. DIRECTION.
C           NFY: NUMBER OF FIBER ELEMENTS IN THE VERT. DIRECTION.
C           NFM: NUMBER OF ELEMENTS IN THE VERT. DIRECTION FROM THE
C                  MODEL MIDPOINT TO THE FIBER END.
C           NEL: NUMBER OF TOTAL ELEMENTS IN THE MODEL (NX x NY).
C           XF: RADIUS OF FIBER DIVIDED BY NFX.
C           XM: (RADIUS OF CELL - RADIUS OF FIBER) DIVIDED BY (NX-NFX).
C           YF1: (LENGTH OF FIBER - 0.5*LENGTH OF CELL) DIVIDED BY NFM.
C           YF2: 0.5*LENGTH OF CELL DIVIDED BY (NFY-NFM).
C           YM: (LENGTH OF CELL - LENGTH OF FIBER) DIVIDED BY (NY-NFY)
C
C PROGRAM CVOL
C PARAMETER (NX=9,NY=27,NFX=6,NFY=18,NFM=4,NEL=243,
C & XF=.1666,XM=.1633,YF1=.19,YF2=.16,YM=.1644)
C      REAL VOL(1:NEL),V(1:NX,1:NY)
C
C INITIALIZE THE MATRICES
C     DO 10 I=1,NX
C     DO 10 J=1,NY
10   V(I,J)=0.0
C
C     DO 15 I=1,NEL
15   VOL(I)=0.0
C
C CONSTRUCT THE V MATRIX AND MAP IT INTO THE VOL MATRIX.
C *** TOP FIBER GROUP ***
NID=1
DO 20 L1=NFY,NFY-NFM+1,-1
DO 21 K1=NFX,1,-1
V(K1,L1)= ((XF*K1)**2 - (XF*(K1-1))**2)*YF1/2.
VOL(NID)=V(K1,L1)
NID=NID+1
21  CONTINUE
20  CONTINUE
C *** BOTTOM FIBER GROUP ***
DO 200 L10=NFY-NFM,1,-1
DO 210 K10=NFX,1,-1
V(K10,L10)= ((XF*K10)**2 - (XF*(K10-1))**2)*YF2/2.
VOL(NID)=V(K10,L10)
NID=NID+1
210 CONTINUE
200 CONTINUE
C *** TOP RIGHT MATRIX ELEMENT GROUP ***
DO 22 L2=NY,NFY+1,-1
DO 23 K2=NX,NFX+1,-1
V(K2,L2)=((XM*(K2-NFX)+XF*NFX)**2-
&          (XM*(K2-1-NFX)+XF*NFX)**2)*YM/2.
VOL(NID)=V(K2,L2)
NID=NID+1
23  CONTINUE
22  CONTINUE
C *** TOP LEFT MATRIX ELEMENT GROUP ***

```

```

DO 24 L3=NY,NFY+1,-1
DO 25 K3=NFX,1,-1
V(K3,L3)= ((XF*K3)**2 - (XF(K3-1))**2)*YM/2.
VOL(NID)=V(K3,L3)
NID=NID+1
25 CONTINUE
24 CONTINUE
C *** MIDDLE MATRIX ELEMENT GROUP ***
DO 26 L4=NFY,NFY-NFM+1,-1
DO 27 K4=NX,NFX+1,-1
V(K4,L4)= ((XM*(K4-NFX)+XF*NFX)**2 -
& (XM*(K4-1-NFX)+XF*NFX)**2)*YF1/2.
VOL(NID)=V(K4,L4)
NID=NID+1
27 CONTINUE
26 CONTINUE
C *** BOTTOM MATRIX ELEMENT GROUP ***
DO 260 L40=NFY-NFM,1,-1
DO 270 K40=NX,NFX+1,-1
V(K40,L40)= ((XM*(K40-NFX)+XF*NFX)**2 -
& (XM*(K40-1-NFX)+XF*NFX)**2)*YF2/2.
VOL(NID)=V(K40,L40)
NID=NID+1
270 CONTINUE
260 CONTINUE
C *** CHECK TO ENSURE THE SUM OF THE ELEMENTAL VOLUMES MATCH THE ***
C *** CALCULATED MODEL VOLUME AND WRITE THE OUTPUT TO A FILE. ***
VNUM= (((XF*NFX)+(XM*(NX-NFX)))**2)*((YF1*NFM) +
& (YF2*(NFY-NFM))+(YM*(NY-NFY)))/2.
C
VCALC=0.0
DO 30 N=1,NEL
VCALC=VCALC+VOL(N)
30 CONTINUE
PRINT *, 'VNUM=' , VNUM
PRINT *, 'VCALC=' , VCALC
DO 35 M=1,NEL
35 WRITE (10,*) VOL(M)
C
STOP
END

C THIS IS A MODIFICATION TO SUBROUTINE READ, WHICH
C CALCULATES STRESS LEVELS ALONG THE FIBER HALF-LENGTH,
C AT GIVEN LOAD LEVELS.
C
SUBROUTINE READ
PARAMETER (NEL=52,LC=1,TVOL=3.0,YFBR=13.0,XFBR=4.0)
REAL SZ(1:NEL,1:4),SZBAR(1:LC),V(1:NEL)
REAL TTFBR(1:LC),STFBR(1:YFBR)
CHARACTER*8 STATE
COMMON // SZ,SZBAR,V,TTFBR,STFBR
C
OPEN (02,STATUS='OLD')
OPEN (03,FILE='FIBER.DAT',STATUS='NEW')
OPEN (04,FILE='FIBER_STRESS.DAT',STATUS='NEW')

```

```

C
DO 15 K=1,LC
OPEN (01,STATUS='OLD')
FSUM=0.0
C
DO 20 M=1,YFBR
SUM=0.0
VOL=0.0
C
DO 25 L=1,XFBR
READ (02,*) IEL
READ (02,21) INR,INS,STATE,SX,SY,SZ(L,1),SYZ,SVM,SMAX
READ (02,*) SYS,SMIN
READ (02,*) 
READ (02,21) INR,INS,STATE,SX,SY,SZ(L,2),SYZ,SVM,SMAX
READ (02,*) SYS,SMIN
READ (02,*) 
READ (02,21) INR,INS,STATE,SX,SY,SZ(L,3),SYZ,SVM,SMAX
READ (02,*) SYS,SMIN
READ (02,*) 
READ (02,21) INR,INS,STATE,SX,SY,SZ(L,4),SYZ,SVM,SMAX
READ (02,*) SYS,SMIN
READ (02,*) 
READ (02,*) 
21 FORMAT (14X,I1,3X,I1,5X,A8,5X,4(E12.5,2X),5X,2(E12.5,4X))
READ (01,*,END=50) V(L)
SBAR=((SZ(L,1)+SZ(L,2)+SZ(L,3)+SZ(L,4))/4.0)*V(L)
SUM=SUM+SBAR
VOL=VOL+V(L)
25 CONTINUE
C
STFBR(M)=SUM/VOL
FSUM=FSUM+SUM
WRITE (03,*) STFBR(M)
20 CONTINUE
C
CLOSE (01)
TTFBR(K)=FSUM/TVOL
WRITE (03,*) 'LOAD STEP=',K
WRITE (04,*) TTFBR(K)
15 CONTINUE
C
CLOSE (02)
50 PRINT*, 'EOF DETECTED'
RETURN
END

```

## LIST OF REFERENCES

1. deSilva, A.R.T., and Chadwick, G.A., *J. Mech. Phys. Solids*, 17 (1969) p. 387.
2. Dvorak, G.J., Rao, M.S.M., and Tarn, J.Q., *J. Comp. Mat.*, 7 (1973), p. 194.
3. Hoffman, C.A., *J. Eng. Mat. Tech.*, 95 (1973), p. 55.
4. Garmong, G., *Met. Trans.*, 5 (1974), p. 2183.
5. Lee, J.K., Earmme, Y.Y., Aaronson, H.I., and Russell, K.C., *Met. Trans.*, 11A (1980), p. 1837.
6. Earmme, Y.Y., Johnson, W.C., and Lee, J.K., *Met. Trans.*, 12A (1981), p. 1521.
7. Arsenault, R.J., and Fisher, R.M., *Scripta Metall.*, 17 (1983), p. 67.
8. Arsenault, R.J., *Mat. Sci. Eng.*, 64 (1984), p. 171.
9. Arsenault, R.J., and Taya, M., *Acta Metall.*, 35 (1987), p. 651.
10. Taya, M., and Arsenault, R.J., *Scripta Metall.*, 21 (1987), p. 349.
11. Nardone, V.C., and Prewo, K.M., *Scripta Metall.*, 20 (1987), p. 349.
12. Arsenault, R.J., and Shi, N., *Mat. Sci. Eng.*, 81 (1986), p. 175.
13. Derby, B., and Walker, J.R., *Scripta Metall.*, 22 (1988), p. 529.
14. Arsenault, L., Wang, L., and Feng, C.R., *Acta Metall.*, 39 (1991), p. 47.
15. Withers, P.J., Stobbs, W.M., and Pederson, O.B., *Acta Metall.*, 37 (1989), p. 3061.
16. Dutta, I., Bourell, D.L., and Latimer, D., *J. Comp. Mat.*, 22 (1988), p. 829.

17. Dutta, I., *Comp. Sci. Tech.*, 41 (1991), p. 193.
18. Povirk, G.L., Needleman, A., and Nutt, S.R., *Mat. Sci. Eng.*, A125 (1990), p. 129.
19. Christman, T., Needleman, A., and Suresh, S., *Acta Metall.*, 31 (1989), p. 3029.
20. Tvergaard, V., *Acta Metall.*, 38 (1990), p. 185.
21. Tvergaard, V., *Mat. Sci. Eng.*, A125 (1990), p. 203.
22. Levy, A., and Papazian, J.M., *Met. Trans.*, 21A (1990), p. 411.
23. Brockenbrough, J.R., and Suresh, S., *Scripta Metall.*, 24 (1990), p. 325.
24. Arsenault, R.J., Shi, N., Feng, C.R., and Wang, L., *Mat. Sci. Eng.*, A131 (1991), p. 55.
25. Arsenault, R.J., and Wu, S.B., *Mat. Sci. Eng.*, 96 (1987), p. 77.
26. Povirk, G.L., Needleman, A., and Nutt, S.R., *Mat. Sci. Eng.*, A132 (1991), p. 31.
27. Sims, J.D., Master's Thesis, Naval Postgraduate School, Monterey, CA, 1990).
28. ADINA Product Manuals, Version 2.0 ADINA R&D Corp., Watertown, MA, December 1987.
29. Takao, Y., Chou, T.W., and Taya, M., *J. Appl. Mech.*, 49 (1982), p. 536.
30. Takao, Y., and Taya, M., *J. Comp. Mat.*, 2 (1987), p. 140.

## **INITIAL DISTRIBUTION LIST**

	No. Copies
1. Defense Technical Information Center Cameron Station Alexandria, VA 22304-6145	2
2. Library, Code 52 Naval Postgraduate School Monterey, CA 93943-5002	2
3. Professor Indranath Dutta, Code ME/Du Department of Mechanical Engineering Naval Postgraduate School Monterey, CA 93943-5100	2
4. LT Dan Seigenthaler 581 B Wilkes Ln. Monterey, CA 93940	2
5. Naval Engineering, Code ME Naval Postgraduate School Monterey, CA 93943-5100	1